

Staggered grids for multidimensional multiscale modelling

J. Divahar ^{*†} A. J. Roberts ^{*‡} Trent W. Mattner ^{*§}
J. E. Bunder ^{*¶} Ioannis G. Kevrekidis ^{||}

July 27, 2022

Abstract

Numerical schemes for wave-like systems with small dissipation are often inaccurate and unstable due to truncation errors and numerical roundoff errors. Hence, numerical simulations of wave-like systems lacking proper handling of these numerical issues often fail to represent the physical characteristics of wave phenomena. This challenge gets even more intricate for multiscale modelling, especially in multiple dimensions. When using the usual collocated grid, about two-thirds of the resolved wave modes are incorrect with significant dispersion. But, numerical schemes on staggered grids (with alternating variable arrangement) are significantly less dispersive and preserve much of the wave characteristics. Also, the group velocity of the energy propagation in the numerical waves on a staggered grid is in the correct direction, in contrast to the collocated grid. For high accuracy and to preserve much of the wave characteristics, *this article extends the concept of staggered grids in full-domain modelling to multidimensional multiscale modelling*. Specifically, this article develops

^{*}School of Mathematical Sciences, University of Adelaide, South Australia.

[†]<https://orcid.org/0000-0002-9506-8846>

[‡]<http://orcid.org/0000-0001-8930-1552>, <mailto:profajroberts@protonmail.com>

[§]<https://orcid.org/0000-0002-5313-5887>

[¶]<http://orcid.org/0000-0001-5355-2288>

^{||}Departments of Chemical and Biomolecular Engineering & Applied Mathematics and Statistics, Johns Hopkins University, Baltimore, Maryland, USA. <https://orcid.org/0000-0003-2220-3522>

120 multiscale staggered grids and demonstrates their stability, accuracy, and wave-preserving characteristic for equation-free multiscale modelling of weakly damped linear waves. But most characteristics of the developed multiscale staggered grids must also hold in general for multiscale modelling of many complex spatio-temporal physical phenomena such as the general computational fluid dynamics.

Contents

1	Introduction	2
2	Collocated and staggered grids for wave-like systems	4
3	Staggered patch grids for equation-free multiscale modelling of waves	8
3.1	Patch coupling connects the scales	8
3.2	Extend the staggered grid to multiscale patch scheme	9
3.3	Multi-layer edge nodes for higher-order spatial derivatives	17
4	Multiscale staggered patch grid for weakly damped linear waves	19
4.1	Derive eigenvalues of a multiscale staggered patch scheme for linear microscale models	21
4.2	Only patch grids with all symmetric patches are stable . . .	26
4.3	Only centred patch grids are accurate	29
5	Conclusion	37

1 Introduction

For wave-like systems with small or no dissipation, accurate numerical simulation is challenging over large spatial scales, especially for long simulation times. Numerical schemes for wave-like systems with small dissipation are often inaccurate and unstable due to numerical dissipation and numerical dispersion caused by truncation and numerical roundoff errors (Hinch 2020, p.136; Zikanov 2010, pp.70–73; Anderson 1995, pp.232–243). Hence, numerical simulations of wave-like systems lacking proper handling of these numerical issues often fail to represent the physical characteristics of wave phenomena. Section 2 overviews using a staggered grid in space for accurate and robust computational simulation of wave-like systems. It is well-known that staggered grids, such as depicted in

Figure 1(right), lead to higher accuracy compared to that of a same order scheme on collocated grids.

Here we develop multiscale staggered grids for wave-like systems in multiple space dimensions—such systems are even more challenging (e.g., see the recent review of modelling materials by Fish et al. (2021)). We expect that for simulations of wave-like systems many of the good characteristics of the usual staggered grids also hold for the multiscale staggered grids. The *Equation-Free Patch scheme* (Kevrekidis and Samaey 2009, e.g.) is a flexible, computationally efficient, multiscale modelling approach. Such patch schemes are an effective and accurate alternative to cognate methods such as the Multiscale Finite Element Method (Altmann et al. 2021; Efendiev et al. 2004; Fish et al. 2021, e.g.). Equation-free multiscale patch schemes have been developed and applied successfully for dissipative systems (Bunder et al. 2017; Maclean et al. 2021; Roberts and Kevrekidis 2005, 2007). Cao and Roberts (2013, 2015) extended the patch scheme to 1D wave-like systems using a staggered macroscale grid of patches in 1D space, where each patch itself contains a staggered microscale grid in 1D space. Here, Section 3 extends and explores the multiscale staggered grids to two-dimensional multiscale modelling (Section 3.2). Extending to higher dimensional space should be straightforward. For wave-like systems in 2D, a total of 167 040 such staggered patch grids are *geometrically compatible* (defined in Section 3.2). We developed and analysed all 167 040 staggered patch grids, among which 120 of them are *centred staggered patch grids* whose sub-patch micro-grids all have a centre node and include a centred-patch corresponding to each of the state variables; the remaining 166 920 are *non-centred patch grids*. For first-order PDEs, the patch schemes over these staggered patch grids interpolate field values to the patch edges. However, higher-order spatial derivatives (e.g., for diffusion) and some nonlinear terms require interpolation to additional layers of edge values (Section 3.3).

Section 4 shows that all the 60 centred multiscale staggered patch grids give stable and accurate equation-free multiscale patch schemes. For representative physical and discretisation parameters, via eigenvalues and wave frequencies, Section 4 demonstrates the stability, accuracy, and wave-preserving characteristic of these centred multiscale staggered grids for weakly damped linear waves. Section 4.2 studies the dependence of the patch scheme stability on the patch grid geometry, the *geometry-stability study*, for all the 167 040 compatible 2D staggered patch grids. The geometry-stability study shows that among all the compatible 167 040 compatible patch grids, only 1248 patch grids (0.75%) whose patches are all symmetric are stable. Section 4.3 shows that none of the non-centred patch grids that are stable (Section 4.2) is accurate. Thus, among all the possible 167 040

compatible 2D staggered patch grids, only 120 centred patch grids (0.07%) are both stable and accurate.

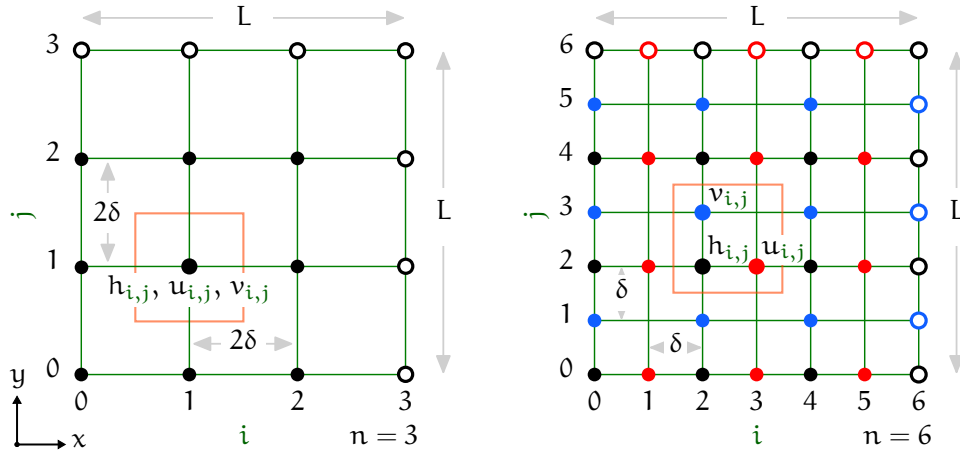
Given the new foundation established here for multidimensional multi-scale staggered grids in the Equation-Free Patch scheme, our subsequent article on multiscale simulation of large-scale linear waves explores two families of patch schemes in detail for their stability, accuracy, and consistency. That forthcoming article also verifies the schemes' insensitivity to numerical roundoff errors. Subsequent articles are planned to develop and explore staggered patch schemes for nonlinear wave PDEs, specifically for the viscous and turbulent shallow water flows. These developments aim to work towards novel, powerful, and efficient computational simulation of the complex multiscale physics of floods, bores, and tsunamis (LeVeque 2015; Reungoat et al. 2018, e.g.).

2 Collocated and staggered grids for wave-like systems

Figure 1(left) depicts an example collocated grid in 2D space, and Figure 1(right) an example 2D staggered grid. In the classification of Arakawa and Lamb (1977, Fig. 3, p.181), these grids are A-grid and C-grid respectively. The collocated grid in Figure 1(left) stores all state variables at each and every discrete point, also called node, at each (i, j) where green grid lines intersect. But the staggered grid in Figure 1(right) intersperses the state variables at alternate discrete points. Here, h, u nodes are horizontally alternating and h, v nodes are vertically alternating. The staggered grid was first used in the Marker and Cell method of Harlow and Welch (1965). Staggered grids were subsequently used in many contexts, including the well-known Semi Implicit Method for Pressure Linked Equations (SIMPLE) of Patankar and Spalding (1972).

Staggered grids preserve much of the wave characteristics (Fornberg and Ghrist 1999, Figs. 8 and 9; Fornberg 1990) and typically support higher accuracy simulations compared to simulations of the same order on collocated grids. For example, even though a central difference scheme on a collocated grid gives second-order accuracy, the same second-order accurate central difference scheme on a staggered grid is significantly less dispersive (Lauritzen et al. 2011, p.46, §3.2; Ólafsson and Bao 2021, p.55, §2.2.1). Furthermore, the group velocity of the energy propagation in the numerical waves on a staggered grid is approximately in the correct direction, whereas on collocated grids the group velocity for large wavenumbers

Figure 1: Schematic *micro-grids*: *collocated grid* on left; *staggered grid* on right where variables are stored only on staggered/alternating discrete points (*nodes* \bullet h , \bullet u , and \bullet v). The collocated grid has 3×3 ($n = 3$) grid intervals in the **green** grid, whereas the staggered grid has 6×6 ($n = 6$) grid intervals, yet both have $3 \times 3 = 9$ micro-cells (**orange** square). The unfilled nodes (\circ , \circ , and \circ) indicate discrete n -periodic boundary values.



is often in the opposite direction (Lauritzen et al. 2011, p.46, §3.2; Ólafsson and Bao 2021, p.55, §2.2.1). When using the usual collocated grid, about two-thirds of the resolved wave modes are incorrect with significant dispersion. For waves in multiple dimensions, such errors in dispersion and group velocity extend over a larger portion of wavenumber space, and so a staggered grid is significantly better than a corresponding scheme on a collocated grid. Staggered grids, such as Figure 1, are simple and robust for numerical simulation of wave-like systems.

We now describe second-order accurate, finite difference schemes for generic 2D wave-like PDEs on both collocated and staggered grids. Consider such a system with little or no dissipation over the periodic spatial domain $[0, L] \times [0, L]$. In terms of state variables $h(x, y, t)$, $u(x, y, t)$, and $v(x, y, t)$, such systems are modelled as non-dimensional wave-like PDEs

$$\frac{\partial h}{\partial t} = -\frac{\partial u}{\partial x} - \frac{\partial v}{\partial y} + \dots, \quad \frac{\partial u}{\partial t} = -\frac{\partial h}{\partial x} + \dots, \quad \frac{\partial v}{\partial t} = -\frac{\partial h}{\partial y} + \dots, \quad (1)$$

with the boundary conditions that the three non-dimensional fields h , u , and v are L -periodic in both the x and y directions. In the generic wave-like PDEs (1), the explicitly written terms (excluding "...") model non-dispersive non-dissipative ideal wave phenomena (Dean and Dalrymple 1991, pp.136–137; Mehaute 1976, p.260). The "..." indicates other linear and/or nonlinear

terms that model additional physical phenomena that modify the wave, such as bed drag, viscous diffusion, turbulent mixing, and surface tension. The dependent variables in PDEs (1) let us interpret the PDEs as a model of water waves with wave height h and horizontal velocities u, v , but the importance of (1) is that it is a generic model of many 2D wave phenomena.

Figure 1(left) depicts the usual *collocated grid*, whereas Figure 1(right) depicts a *staggered grid* for typical simulations of generic wave-like systems modelled by PDEs (1). The grids in Figure 1 are termed *micro-grids* in order to distinguish them from the macro-grids created for our multiscale modelling (Section 3). Figure 1 shows the collocated grid with 3×3 ($n = 3$) grid intervals, and the staggered grid with 6×6 ($n = 6$) grid intervals, yet both these grids contain $3 \times 3 = 9$ *micro-cells* (one micro-cell is depicted by an orange square). In both collocated and staggered grids, each micro-cell contains all three state variables $h_{i,j}$, $u_{i,j}$, and $v_{i,j}$. In general, for any positive even number n , a collocated grid with $n/2 \times n/2$ grid intervals and a staggered grid with $n \times n$ grid intervals, have the same number of micro-cells, namely $n/2 \times n/2 = n^2/4$, and the same number of state variables, namely $3n^2/4$. The unfilled nodes (\circ , \circ , and \circ) on the boundaries of the two grids in Figure 1 schematically indicate discrete n -periodic boundary values.

Consider the collocated grid of Figure 1(left) with n grid intervals, each 2δ -wide in both x and y directions (e.g., $n = 3$ for the specific collocated grid of Figure 1(left)). Approximating the spatial derivatives in the wave-like PDEs (1) on the nodes of the collocated grid (e.g., filled markers of Figure 1(left)) by central finite differences gives the *collocated microscale model* (for $i, j \in \{0, 1, 2, \dots, n-1\}$)

$$\bullet \frac{dh_{i,j}}{dt} = -\frac{u_{i+1,j} - u_{i-1,j}}{4\delta} - \frac{v_{i,j+1} - v_{i,j-1}}{4\delta} + \dots, \quad (2a)$$

$$\bullet \frac{du_{i,j}}{dt} = -\frac{h_{i+1,j} - h_{i-1,j}}{4\delta} + \dots, \quad (2b)$$

$$\bullet \frac{dv_{i,j}}{dt} = -\frac{h_{i,j+1} - h_{i,j-1}}{4\delta} + \dots. \quad (2c)$$

Similarly, consider the staggered grid in Figure 1(right) with n grid intervals each δ -wide in both x and y directions (e.g., $n = 6$ for the specific staggered grid of Figure 1(right)). Approximating the spatial derivatives in the generic wave-like PDEs (1) on the nodes (e.g., filled markers of Figure 1(right)) by central finite differences gives the *staggered microscale model* (for $i, j \in$

$\{0, 1, 2, \dots, n-1\}$)

$$\bullet \frac{dh_{i,j}}{dt} = -\frac{u_{i+1,j} - u_{i-1,j}}{2\delta} - \frac{v_{i,j+1} - v_{i,j-1}}{2\delta} + \dots \quad i, j \text{ even}, \quad (3a)$$

$$\bullet \frac{du_{i,j}}{dt} = -\frac{h_{i+1,j} - h_{i-1,j}}{2\delta} + \dots \quad i \text{ odd}, \quad j \text{ even}, \quad (3b)$$

$$\bullet \frac{dv_{i,j}}{dt} = -\frac{h_{i,j+1} - h_{i,j-1}}{2\delta} + \dots \quad i \text{ even}, \quad j \text{ odd}. \quad (3c)$$

The “...” in the collocated and staggered grid models (2) and (3) indicate discrete approximations of other linear and/or nonlinear terms corresponding to the “...” in the generic wave-like PDEs (1). The coloured bullets \bullet , \bullet , \bullet in the microscale models (2) and (3) indicate the h , u , and v nodes, respectively.

Corresponding to the periodic boundary conditions of the generic wave-like PDEs (1), in the collocated and staggered grid models (2) and (3) the three fields h , u , v are n -periodic in both i and j , where $n = L/(2\delta)$ for the collocated grid and $n = L/\delta$ for the staggered grid.

The PDEs (1) inspire the microscale computational models (2) and (3). But, the aim of our multiscale patch schemes is to accurately compute the solutions of the microscale computational model, not the solutions of the PDEs. Thus, how well the microscale discretisations (2) and (3) predict the solutions of the PDEs (1) is a peripheral issue for this article.

Arranging the state variables of the microscale model (2) defined on the *nodes* of the collocated grid in Figure 1(left), namely $\bullet h_{i,j}$, $\bullet u_{i,j}$, and $\bullet v_{i,j}$, into a vector gives the *state vector of the collocated microscale model* \mathbf{x} . Similarly, arranging the state variables of the microscale model (3) defined on the *nodes* of the staggered grid in Figure 1(right), namely $\bullet h_{i,j}$, $\bullet u_{i,j}$, and $\bullet v_{i,j}$, into a vector gives the *state vector of the staggered microscale model* \mathbf{x} . In terms of the state vector \mathbf{x} , both the collocated and staggered microscale models (2) and (3) are represented as a dynamical system by the ODEs

$$\frac{d\mathbf{x}}{dt} = \mathbf{f}(\mathbf{x}), \quad (4)$$

where the microscale model \mathbf{f} is a vector function encapsulating the spatially discrete model, such as the equations (2) or (3), for the generic wave-like PDEs (1). A full-domain microscale simulation is performed by numerical time-integration of the ODEs (4)—the spatially discrete microscale model (2) or (3)—on the nodes of the collocated/staggered micro-grid (filled markers in Figure 1).

3 Staggered patch grids for equation-free multiscale modelling of waves

This section extends the concept of 2D staggered grids (Section 2) to multiscale modelling by developing *2D staggered patch grids* for equation-free multiscale modelling (Cao and Roberts 2015; Kevrekidis and Samaey 2009, e.g.). A further extension to 3D should be straightforward.

In the equation-free multiscale framework, a patch scheme performs detailed microscale simulations within small, widely separated, *patches* of space (e.g., the small violet squares enclosing green grid in Figure 3a), and couples the patches (*patch coupling*) via interpolation over the macroscale space between the patches (Hyman 2005; Kevrekidis et al. 2004; Kevrekidis and Samaey 2009). One can achieve arbitrarily high orders of macroscale consistency for patch schemes via appropriate high order interpolation for the patch coupling (Bunder et al. 2021; Roberts and Kevrekidis 2005, 2007). For development and analysis of the staggered patch grids, throughout this article we use *spectral interpolation* (Bunder et al. 2020, §2.2.3), via Fourier transforms, to couple patches.

Section 3.2 explains extending 2D staggered grids over a full-domain to multiscale modelling, using a 2D staggered macroscale grid of patches and a 2D staggered *micro-grid* within each patch. The discussion in Section 3.2 is for PDEs with only first order derivatives. Section 3.3 explains extending the 2D staggered grid to multiscale modelling for linear/nonlinear PDEs with higher-order and mixed derivatives. Section 4 then determines which of the many possible staggered patch grids give stable and accurate patch schemes for linear waves (1).

3.1 Patch coupling connects the scales

In an equation-free multiscale patch scheme, patch coupling gives the patch edge values (unfilled circles on the patch edges in Figure 3a), via two steps:

1. for each patch compute a representative *macroscale patch value* (also called aggregate value, amplitude or order parameter) from the patch's respective microscale interior values;
2. compute the *microscale* edge values of each patch by interpolating from the macroscale patch values of neighbouring patches across the relatively large inter-patch distances.

In this way, patch coupling provides a two-way connection between the microscale and macroscale.

Patch coupling using polynomial or spectral interpolation leads to two broad families of patch schemes. To focus on the issue of the geometric design of the multiscale patch scheme, throughout this article we use the highly accurate spectral interpolation to provide the edge values (Bunder et al. 2020, §2.2.3). In summary, at each time one first computes the 2D Fourier transform of the patch's aggregate values. Second, for each edge position, simultaneously over all patches, one uses the Fourier shifting property, and an inverse 2D Fourier transform, to compute all the required edge values. This spectral patch coupling was found to be highly accurate in *one* possible design of a 2D staggered patch scheme (Bunder et al. 2020, §2.2.4).

In a patch scheme, at each time step, the edge values (by the patch coupling) and the interior node values (from the previous time step) are known. Given the edge values and the interior values at the current time step, an ODE integrator such as BS3 of `DifferentialEquations.jl` (Rackauckas and Nie 2017), computes the interior values at the next time step by computing time derivatives from the governing ODEs, such as the ODEs (3).

Patch schemes essentially provide a reduced order multiscale model of the given corresponding microscale model. The macroscale (aggregate) values of patches would then usually be state variables in a slow manifold of the patch scheme (Roberts 2003, §5.3, p.302; Kevrekidis et al. 2004, p.1349; Zagaris et al. 2009; Roberts 1988; Foias et al. 1988a; Lorenz 1986; Foias et al. 1988b; Temam 1990). Our aim for designing patch schemes is that the scheme should have both the following properties: have a slow manifold that accurately matches the slow dynamics of the given microscale model; and the scheme should be stable.

3.2 Extend the staggered grid to multiscale patch scheme

To take advantage of the 'wave-friendly' features of staggered grids (Section 2), here we adapt and extend the collocated patch scheme previously established for dissipative systems (Bunder et al. 2017; Maclean et al. 2021; Roberts and Kevrekidis 2005, 2007). Figure 3a shows one example staggered grid of patches, in 2D there are a total of 167 040 such staggered patch grids possible. The following list defines the parameters for such staggered patch grids composed of square patches distributed over a square macroscale domain.

- *Macro-grid interval* Δ , also *inter-patch distance*, is the distance between two adjacent patch centres (size of the violet grid intervals) in x -

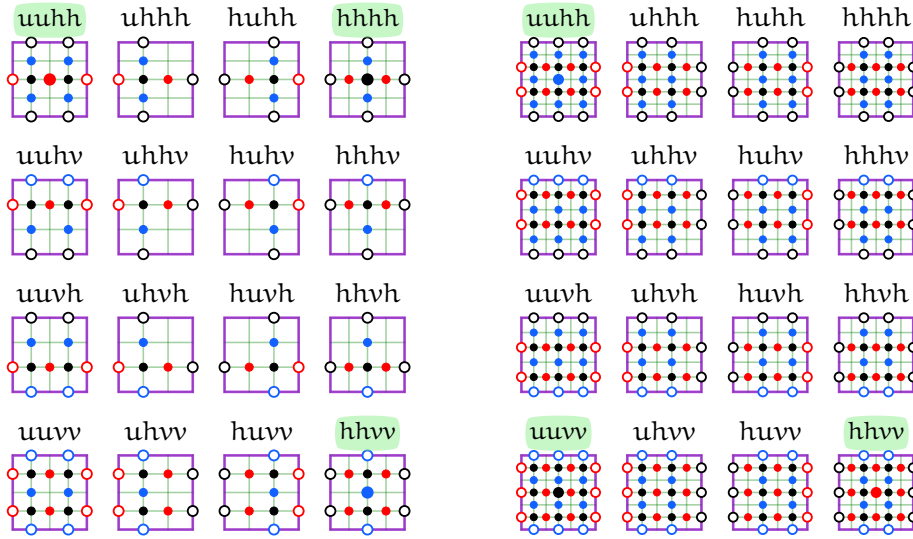
and y -directions (we focus on *uniformly spaced patches* over a square domain).

- *Number of macro-grid intervals* N is the number of grid intervals (**violet**) in the periodic domain in each of the x - and y -directions.
- *Sub-patch micro-grid interval* δ is the distance between two adjacent micro-grid nodes (size of the **green** grid intervals) in each of the x - and y -directions (we focus on *uniformly spaced micro-grid nodes*).
- *Number of sub-patch micro-grid intervals* n is the number of microscale grid intervals (**green**) within a square patch in each of the x - and y -directions.
- *Patch size* l is the side length of the square patch (**violet** squares enclosing **green** grid) in x - and y -directions.
- *Patch scale ratio* $r = l/(2\Delta)$ quantifies the ratio of the simulated to the unsimulated space for each spatial dimension. In practical use, patch scale ratios $r = l/(2\Delta)$ are small, typically ranging from 0.0001 to 0.1.

For a patch scheme over a collocated patch grid, constructing and using a collocated micro-grid (Figure 1, left) within a patch is straightforward as there is only one way to arrange patch edge nodes. But when we invoke a staggered micro-grid (Figure 1, right) within a patch (the small **violet** squares enclosing **green** grid in Figure 3a), the heterogeneous nodes lead to many possible arrangements for the patch edge nodes. The type of edge nodes (h , u , or v) on left, right, bottom and top edges on a patch edge define the *edge type* of that patch. We identify a *patch type*, or equivalently a sub-patch *micro-grid type*, by its edge type. For example, the patch type (or the micro-grid type) $uuvv$ in the left-bottom of Figures 2a and 2b has u -edge nodes on left and right edges, and v -edge nodes on bottom and top edge nodes. To simplify the organisation and discussion, micro-grids with 4 or 3 sub-patch micro-grid intervals are both identified by $n = 4$ as in Figure 2a, similarly micro-grids with 6 or 5 sub-patch micro-grid intervals are identified by $n = 6$ as in Figure 2b. But there is no ambiguity as the edge type uniquely identifies them. When a patch contains a centre node (**green** highlighted names in Figures 2a and 2b), we call it a *centred patch*, otherwise a *non-centred patch*. This *centredness* depends on both the patch edge type and whether $n/2$ is odd or even. For example, the $uuvv$ patch is non-centred (Figure 2a, left-bottom) for $n = 4$ (i.e., even $n/2$), but the same $uuvv$ patch is centred (Figure 2b, left-bottom) for $n = 6$ (i.e., odd $n/2$). We also identify a centred patch by its centre node. For example, in Figure 2b

Figure 2: All 16 possible geometrically compatible staggered sub-patch micro-grids (patches) for PDEs (3) of wave-like systems, with $n = 4, 6$ sub-patch micro-grid intervals. Names indicate the node type on left, right, bottom, and top edges respectively. Patches with green highlighted names have centred nodes. Centredness depends on both the edge type and whether $n/2$ is odd or even.

- (a) Staggered micro-grids for $n = 4$ (i.e., even $n/2$). The patches $h h h h$, $u u h h$, and $h h v v$ are h -, u -, and v -centred patches respectively.
- (b) Staggered micro-grids for $n = 6$ (i.e., odd $n/2$). The patches $u u h h$, $h h v v$, and $u u h h$ are h -, u -, and v -centred patches respectively.



for $n = 6$, the $u u v v$, $h h v v$, and $u u h h$ patches are also called h -, u -, and v -patches respectively. Except where explicitly stated, the details in this article are mainly given for the case of $n = 6$ sub-patch micro-grid intervals.

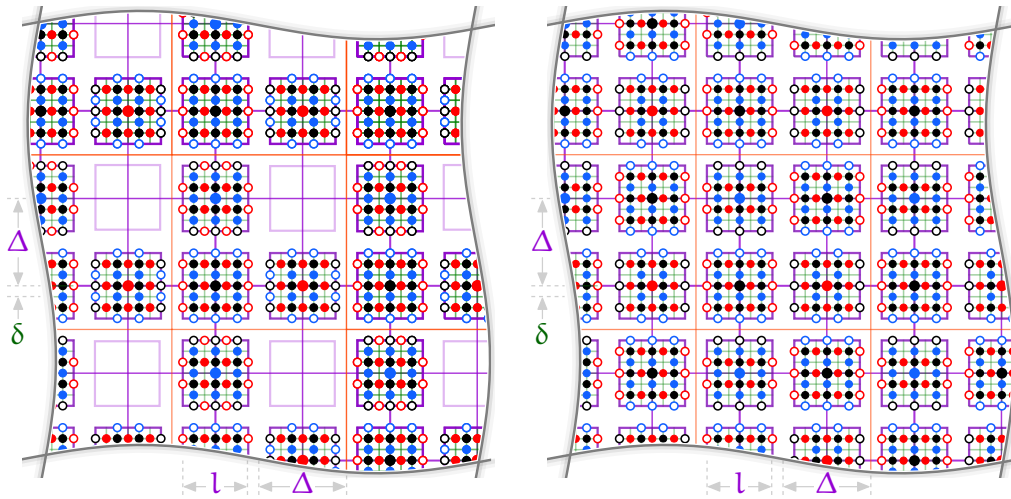
We define a staggered micro-grid to be *geometrically compatible* if it has all the necessary edge nodes (unfilled markers in Figure 2) to calculate all the finite differences of the specified ODEs (3) at all the interior nodes. Figure 2 shows all 16 possible geometrically compatible staggered sub-patch micro-grids (i.e., patches). For example, the $u h v v$ micro-grid (second in the bottom row of Figure 2b) would not be compatible if the right edge all contains \circ v -nodes instead of \circ h -nodes, as the \circ h -nodes on the right edge are necessary to compute $\partial h / \partial x$ on the right most interior \bullet u -nodes.

Consider a possible 2D staggered patch grid to be designed, comprising the macro-cells (orange squares in Figure 3a) each containing $2 \times 2 = 4$ possible patches (violet squares enclosing green micro-grid in Figure 3a).

Figure 3: Example staggered patch grids for $n = 6$ sub-patch micro-grid intervals with three (left) and four patches (right) per macro-cell. The patch grid parameters are patch size l , macro-grid interval Δ , sub-patch micro-grid interval δ . The patches here are enlarged for visual clarity; in practice the patches are very small relative to their inter-patch distance Δ , with small patch scale ratio $r = l/(2\Delta)$ roughly ranging from 0.0001 to 0.1.

(a) Patch grid #79985, using three patches $uuvv$, $hhvv$ and $uuhh$, gives stable and accurate patch schemes with minimal computation. This patch grid is the central focus of this article.

(b) Patch grid #80001, using four patches $uuvv$ (twice), $hhvv$, and $uuhh$, also gives stable and accurate patch schemes, but with more computation than #79985.



These macro-cells in a patch grid are on the macroscale similar to the micro-cells in a micro-grid (orange square in Figure 1) on the microscale. Similar to the $n^2/4$ micro-cells in a $n \times n$ full-domain micro-grid¹ (Section 2), there are $N^2/4$ macro-cells in a $N \times N$ staggered patch grid. Each of the four patches within a macro-cell could be either empty or contain one of the 16 possible micro-grids of Figure 2 depending upon whether $n/2$ is odd or even. Thus, excluding the all-empty case, in a 2×2 macro-cell configuration, the total number of possible 2D staggered patch grids is $(16 + 1)^4 - 1 = 83\,520$ for each n . Including all the 32 possible sub-patch micro-grids in Figure 2 for any number of sub-patch micro-grid intervals n , there are a total of 167 040 possible 2D staggered patch grids. We analysed all of these 167 040 staggered patch grids. For each of the two cases of $n/2$

¹We use the same symbol n and δ for both the full-domain micro-grid and the sub-patch micro-grid, and disambiguate by words and/or context.

being odd or even, this article separately analyses the respective 83 520 staggered patch grids, covering the total of 167 040 patch grids. We uniquely identify each of these 83 520 staggered patch grids for a particular n using a base 17 number whose decimal equivalent, *patch grid Id*, ranges from #1 to #83520. For a particular n , each of the 17 digits encodes either an empty patch or one of the 16 possible sub-patch micro-grids in [Figure 2](#). The magnitude of these numbers does not have any significance, but the closer these numbers the more similar the patch grid geometries are. For example, [Figure 3](#) shows two staggered patch grids with Ids #79985 and #80001; these two patch grids are nearly the same except for an additional h-centred patch in each macro-cell for the #80001 patch grid.

Based on the centredness of the sub-patch micro-grids (green highlighted in [Figure 2](#)), there are two types of qualitatively different staggered patch grids:

- *centred staggered patch grids* whose sub-patch micro-grids all have a centre node and include a centred-patch corresponding to each of the state variables;
- staggered patch grids that are not centred staggered patch grids are *non-centred staggered patch grids*.

For example, for $n = 6$ the two patch grids in [Figure 3](#), #79985 and #80001, are both centred patch grids. But in [Figure 3](#) replacing any of the centred patch or the empty patch with a non-centre patch gives a non-centred patch grid. Even when all sub-patch micro-grids have a centre node, if a patch grid does not contain a centred-patch corresponding to each of the state variables, it is not a centred patch grid. For example, replacing all the centred patches in [Figure 3a](#) with any one particular centred patch, say all-h-centred patches, gives a non-centred patch grid. For patches without a centre node, we compute the macroscale patch value by averaging over the closest respective h, u, v values to the patch centre. It is these macroscale patch values that are used in coupling the patches ([Section 3.1](#)).

In [Figure 3a](#) with three non-empty patches, any of the 24 permutations of the $h-, u-, v$ -patches or an empty patch is also a centred patch grid as per the definition. Hence, for a given n there are 24 centred staggered patch grids containing three patches per cell. In [Figure 3b](#) with four non-empty patches, any of the 12 unique permutations of the $h-, u-, v$ -patches with repeated h -patch is also a centred patch grid. A similar patch grid with a repeated u -patch or a repeated v -patch has 12 unique permutations of centred patch grids. Hence, for a given n there are 36 centred staggered patch grids containing four patches per cell. So, for a given n , among the

83 520 staggered patch grids, $24 + 36 = 60$ of them are centred staggered patch grids containing either three or four patches per cell; and the remaining 83 460 are non-centred patch grids. Thus, for both the cases of $n/2$ being odd or even, in total there are 120 centred staggered patch grids and 166 920 non-centred patch grids.

Whereas all the possible 167 040 staggered patch grids are geometrically compatible 2D discretisations for simulating multiscale wave physics, most of them constitute unstable patch schemes (Section 4.2). The geometry-stability study of Section 4.2 shows that *almost all non-centred staggered patch grids lead to unstable patch schemes but all centred patch grids constitute stable patch schemes*. The accuracy study of Section 4.3 shows that all the centred staggered patch grids constitute accurate patch schemes and that none of the stable non-centred patch grids constitutes accurate patch schemes. That is, only the 120 centred staggered patch grids among all the 167 040 compatible staggered patch grids constitute stable and accurate multiscale patch schemes. All 120 centred staggered patch grids that constitute stable patch schemes are with the same accuracy (Section 4.3), yet due to fewer nodes, the 48 centred patch grids with three patches per macro-cell cost less computation compared to the remaining 72 centred patch grids with four patches per macro-cell.

The staggered patch grid #79985 in Figure 3a is the main example for the specific discussions in this article.

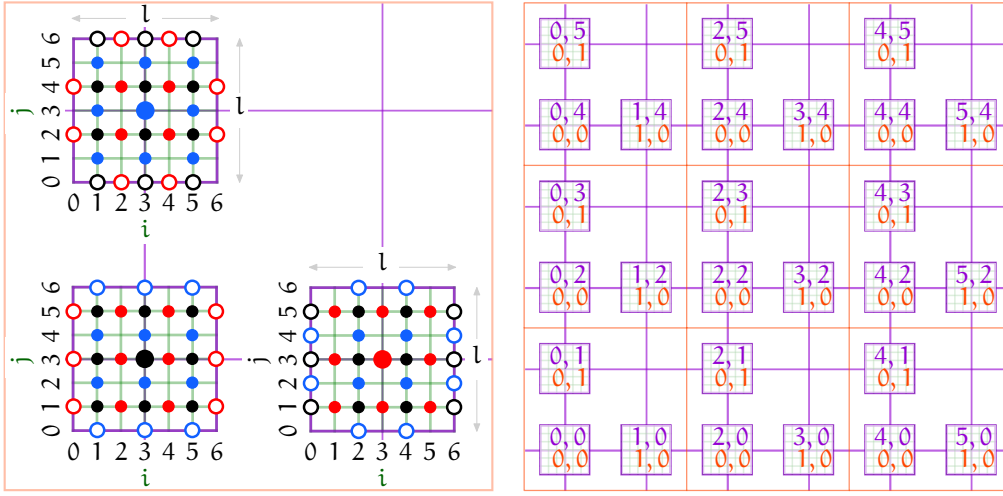
Figure 4 illustrates the following three kinds of indices we use to identify patches and sub-patch micro-grid nodes in all cases, using the staggered patch grid #79985 in Figure 3a as a specific example:

- the pair $I, J \in \{0, 1, \dots, N - 1\}$ is the global (macroscale) patch index;
- the pair p, q , defined by $p := I \bmod 2$ and $q := J \bmod 2$, is the local (macroscale) sub-cell patch index, that is, $p, q \in \{0, 1\}$ within each macro-cell (orange squares in Figure 4b);
- the pair i, j is the sub-patch micro-grid node index, with $i, j \in \{1, \dots, n - 1\}$ for interior nodes (filled markers $\bullet, \color{red}\bullet, \color{blue}\bullet$ in Figure 4a) and $i, j \in \{0, n\}$ for patch edge nodes (unfilled markers $\circ, \color{red}\circ, \color{blue}\circ$ in Figure 4a).

Using the microscale model (3) within the patches in a staggered patch grid (Figure 3a) with N macro-grid intervals (i.e., total of $N/2 \times N/2$ macro-cells), where each patch consists of $n \times n$ sub-patch micro-grid intervals (e.g., $n = 6$ in Figure 3a), gives the *staggered patch scheme* for the microscale model (3) of a generic wave-like system as the following in the specific case

Figure 4: Index convention, using the patch grid #79985 in Figure 3a as a specific example, but the same convention is used for all the 167 040 compatible 2D staggered patch grids. Here, the staggered patch grid has $N = 6$ macro-grid intervals (violet), containing staggered patches of staggered micro-grids with $n = 6$ micro-grid intervals (green).

- (a) Sub-patch micro-grid node index $i, j \in \{1, 2, \dots, n-1\}$ for the interior nodes (\bullet, \circ, \circ) and $i, j \in \{0, n\}$ for patch edge nodes (\circ, \circ, \circ). (b) Global (macroscale) patch index $I, J \in \{0, 1, \dots, N-1\}$; local sub-cell patch index $p, q \in \{0, 1\}$ within each macro-cell (orange squares).



of Figure 3a (with $i, j \in \{1, \dots, n-1\}$):

$$\bullet \frac{d}{dt} h_{i,j}^{I,J}(t) = -\frac{u_{i+1,j}^{I,J} - u_{i-1,j}^{I,J}}{2\delta} - \frac{v_{i,j+1}^{I,J} - v_{i,j-1}^{I,J}}{2\delta} + \dots, \quad (5a)$$

$i - p$ odd, $j - q$ odd;

$$\bullet \frac{d}{dt} u_{i,j}^{I,J}(t) = -\frac{h_{i+1,j}^{I,J} - h_{i-1,j}^{I,J}}{2\delta} + \dots, \quad i - p \text{ even}, \quad j - q \text{ odd}; \quad (5b)$$

$$\bullet \frac{d}{dt} v_{i,j}^{I,J}(t) = -\frac{h_{i,j+1}^{I,J} - h_{i,j-1}^{I,J}}{2\delta} + \dots, \quad i - p \text{ odd}, \quad j - q \text{ even}; \quad (5c)$$

and a patch coupling computes the edge values $\circ h_{i,j}^{I,J}$, $\circ u_{i,j}^{I,J}$, and $\circ v_{i,j}^{I,J}$ for

$$\begin{aligned} & i \in \{0, n\} \text{ for left and right edges, } j \in \{0, n\} \text{ for bottom and} \\ & \text{top edges, } I \text{ even for } h, v, \quad I \text{ odd for } u, \quad J \text{ even for } h, u, \quad J \\ & \text{odd for } v. \end{aligned} \quad (5d)$$

Due to the chosen periodic boundary conditions for the full-domain micro-scale model (3), the three fields h, u, v are macroscale N -periodic in both I

and J , where $N = L/\Delta$. A specific patch coupling method computes patch edge nodes ($\circ h_{i,j}^{I,J}$, $\circ u_{i,j}^{I,J}$, $\circ v_{i,j}^{I,J}$ in Figure 3a) from the aggregate values of the neighbouring patches ($\bullet h_{i,j}^{I,J}$, $\bullet u_{i,j}^{I,J}$, $\bullet v_{i,j}^{I,J}$ with $i = j = n/2$ in the case of Figure 3a). The patch coupling provides the mechanism whereby patches influence each other.

Arranging the patch interior values of the scheme (5), which are over the staggered patch grid such as in Figure 4, into a vector gives the state vector \mathbf{x}^I of the staggered patch scheme, which is a dynamic state variable evolving in time. Here the superscript $(\cdot)^I$ is not an index or exponent, instead, a qualifier denoting the patch interior nodes. In the specific case of Figure 4, the staggered patch scheme state vector

$$\mathbf{x}^I = (h_{1,1}^{0,0}, h_{1,3}^{0,0}, \dots, u_{2,1}^{0,0}, u_{2,3}^{0,0}, \dots, v_{1,2}^{0,0}, v_{1,4}^{0,0}, \dots, h_{1,2}^{0,1}, h_{1,4}^{0,1}, \dots, u_{2,2}^{0,1}, u_{2,4}^{0,1}, \dots, v_{1,1}^{0,1}, v_{1,3}^{0,1}, \dots, h_{1,1}^{0,2}, h_{1,3}^{0,2}, \dots, u_{2,1}^{0,2}, u_{2,3}^{0,2}, \dots, v_{1,2}^{0,2}, v_{1,4}^{0,2}, \dots, h_{2,1}^{1,0}, h_{2,3}^{1,0}, \dots, u_{1,1}^{1,0}, u_{1,3}^{1,0}, \dots, v_{2,2}^{1,0}, v_{2,4}^{1,0}, \dots, h_{2,1}^{1,2}, h_{2,3}^{1,2}, \dots, u_{1,1}^{1,2}, u_{1,3}^{1,2}, \dots, v_{2,2}^{1,2}, v_{2,4}^{1,2}, \dots, h_{1,1}^{0,2}, h_{1,3}^{0,2}, \dots, u_{2,1}^{0,2}, u_{2,3}^{0,2}, \dots, v_{1,2}^{0,2}, v_{1,4}^{0,2}, \dots).$$

Here, the total number of patch interior nodes, the size of the state vector \mathbf{x}^I ,

$$n_p^I := (N^2/4)(9n^2/4 - 4n + 2), \quad (6)$$

where N is the number of macro-grid intervals and n is the number of sub-patch micro-grid intervals. For example, for $N = 6, 10, 14, 18, 22, 26$ macro-grid intervals with $n = 6$ sub-patch micro-grid intervals, $n_p^I = 531, 1475, 2891, 4779, 7139, 9971$ respectively. This n_p^I is only for the 48 centred patch grids with three patches per macro-cell, the 72 centred patch grids with four patches per macro-cell have more interior nodes.

Arranging the patch edge values of the staggered patch scheme (5), with $i, j \in \{0, n\}$ for Figure 4, into a vector gives the edge vector \mathbf{x}^E , of size n_p^E , containing all the edge values of all the patches. The edge vector \mathbf{x}^E is a function of the state vector \mathbf{x}^I —a function $\mathbf{x}^E(\mathbf{x}^I)$ determined by the patch coupling of a particular patch scheme.

Using a multiscale staggered patch grid with one layer of edge nodes, such as in Figure 3, allows for calculating the first spatial derivatives on all patch interior nodes. For ideal waves modelled by PDEs (1), after dropping the additional terms denoted by "...", a staggered patch grid with one layer of edge nodes is sufficient as in Figures 3 and 4a. The staggered sub-patch micro-grids in Figure 3 are also sufficient for many other wave PDEs containing only first-order spatial derivatives. Multiscale staggered grid discretisation of more complex terms in the PDEs (1) often requires additional layers of edge nodes (Section 3.3). For the specific multiscale staggered patch grid in Figure 3a, the total number of patch edge nodes, the

size of the edge vector \mathbf{x}^E , is $n_p^E := (N^2/4)(5n-4)$, where N is the number of macro-grid intervals and n is the number of sub-patch micro-grid intervals. For example, for the staggered patch grid in [Figure 3a](#) with $N = 6, 10, 14, 18, 22, 26$, and $n = 6$, $n_p^E = 360, 1000, 1960, 3240, 4840, 6760$ respectively. The 72 centred patch grids with four patches per macro-cell have more edge nodes.

In terms of the state vector \mathbf{x}^I and the edge vector function $\mathbf{x}^E(\mathbf{x}^I)$, a staggered patch scheme (5) is represented as a dynamical system by ODEs of the form

$$\frac{d\mathbf{x}^I}{dt} = \mathbf{F}(\mathbf{x}^I; \mathbf{x}^E(\mathbf{x}^I)). \quad (7)$$

The $\mathbf{F}(\mathbf{x}^I; \mathbf{x}^E(\mathbf{x}^I))$ in the ODEs (7) corresponds to the $\mathbf{f}(\mathbf{x})$ in the microscale model (4). The functions \mathbf{F} and \mathbf{f} encode the same microscale model for the generic wave-like system (1), except for the following difference: the only argument of \mathbf{f} is the nodal values \mathbf{x} in the full-domain micro-grid; whereas the two arguments of \mathbf{F} are the patch interior values \mathbf{x}^I and the patch edge values $\mathbf{x}^E(\mathbf{x}^I)$ from the patch coupling.

A staggered patch scheme simulation is performed by numerical time-integration of the ODEs (7) for the particular staggered microscale ODEs (5) on the interior nodes of the patches (e.g., filled markers in [Figures 3a](#) and 5), with some particular patch coupling represented by $\mathbf{x}^E(\mathbf{x}^I)$.

3.3 Multi-layer edge nodes for higher-order spatial derivatives

The staggered patch grids of [Figure 3](#) are suitable for PDEs with only first order spatial derivatives, such as PDEs (1) with “+ . . .” omitted. However, sub-patch microscale discretisations of higher-order spatial derivatives (such as second spatial derivative for viscous diffusion) need to use a wider stencil of nodes on the micro-grid. A wider stencil is not an issue for most of the interior nodes, but the interior nodes closest to the edges of a patch need values of nodes that lie outside the sub-patch micro-grids in [Figure 3](#).

As a prototypical example of wave-like PDEs (1) with high-order derivatives, we consider the non-dimensional *weakly damped linear wave* PDEs

$$\frac{\partial h}{\partial t} = -\frac{\partial u}{\partial x} - \frac{\partial v}{\partial y}, \quad (8a)$$

$$\frac{\partial u}{\partial t} = -\frac{\partial h}{\partial x} - c_D u + c_V \frac{\partial^2 u}{\partial x^2} + c_V \frac{\partial^2 u}{\partial y^2}, \quad (8b)$$

$$\frac{\partial v}{\partial t} = -\frac{\partial h}{\partial y} - c_D v + c_V \frac{\partial^2 v}{\partial x^2} + c_V \frac{\partial^2 v}{\partial y^2}, \quad (8c)$$

with linear drag and viscous diffusion respectively characterised by the coefficients c_D, c_V . The macroscale boundary conditions remain that the three fields $h, u,$ and v are L -periodic in both x and y . The case $c_D = c_V = 0$ corresponds to the non-dissipative *ideal wave* PDEs (Dean and Dalrymple 1991, pp.136–137; Mehauté 1976, pp.257–258). General solutions of the PDEs (8) are linear combinations of progressive sinusoidal waves that decay at rates depending upon c_D and c_V .

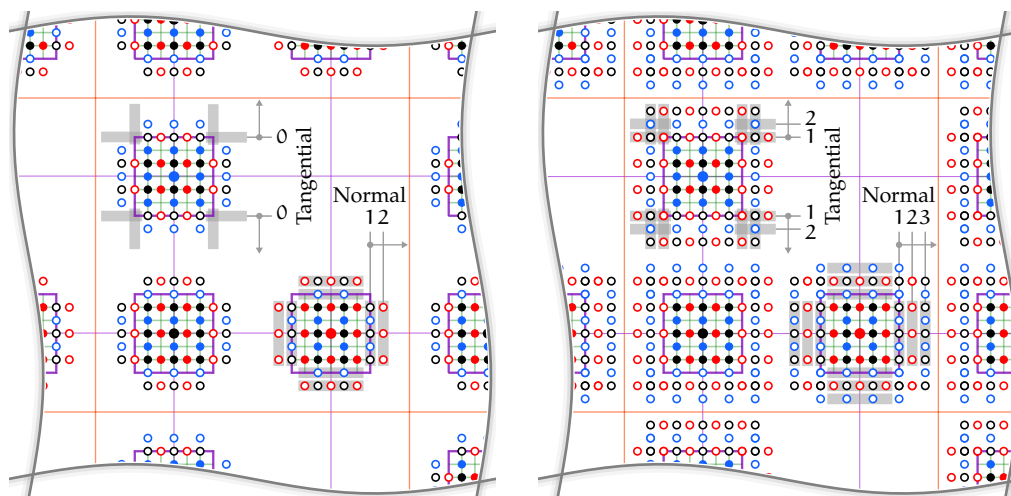
We explored the following two families of methods of approximating the second derivatives in (8) on the micro-grids inside each patch.

- This first methods was unsuccessful. Whenever the microscale finite difference model needs nodes outside the patch edges, we used the nearest edge and interior nodes to extrapolate the required outside node values (we tried constant values, linear and quadratic extrapolation). In effect, such extrapolations change the centred finite differences, such as in (5), into non-centred finite differences for the interior nodes close to the edge nodes. But it eventuated that such extrapolation makes most variants of the staggered patch schemes unstable.
- A successful alternative method that we developed is to append additional layers of edge nodes to the sub-patch micro-grid as in Figures 5a and 5b. We calculate the values of these extra edge layer nodes using the same spectral interpolation as in calculating the edge values of Figure 3a. Unlike the first method using extrapolation, this method uses the same spatial finite difference formula at all interior nodes within each patch, including those close to the edge nodes. Section 4 shows this method of additional layers of edge nodes gives good families of stable and accurate patch schemes.

Figure 5 shows two example staggered patch grids with additional layers of edge nodes. Irrespective of the number of layers of the edge nodes, the staggered patch grids contain the same number of patch interior nodes for a given number of sub-patch micro-grid intervals (e.g., $n = 6$ in Figures 3 and 5). For finite difference approximation of all the terms in the PDEs (8), a staggered patch grid in Figure 5a is sufficient (Section 4.1). For Figure 5a with two layers of edge nodes in the normal direction to the edges and no edge nodes in the tangential direction to the edges, the left and right edge values are $\circ h_{i,j}^{I,J}, \circ u_{i,j}^{I,J}, \circ v_{i,j}^{I,J}$, for $i \in \{-1, 0, n, n + 1\}$ and $j \in \{1, 2, \dots, n - 1\}$. Similarly the bottom and top edge value indices are $i \in \{1, 2, \dots, n - 1\}$ and $j \in \{-1, 0, n, n + 1\}$.

Figure 5: Centred staggered patch grid #79985 of Figure 3a with the same grid parameters but with additional multi-layer edge nodes, contain the same number of interior nodes $\bullet h_{i,j}^{I,J}$, $\bullet u_{i,j}^{I,J}$, $\bullet v_{i,j}^{I,J}$ for $i, j \in \{1, \dots, n-1\}$. But the number of edge values $\circ h_{i,j}^{I,J}$, $\circ u_{i,j}^{I,J}$, and $\circ v_{i,j}^{I,J}$ depend on the number of layers of edge nodes. Layer numbers are shown for the right edge.

- (a) Two layers of edge nodes in normal direction to the edges, no edge nodes in tangential direction to the edges (e.g., no $\bullet v$ node on corners of $\bullet u$ -centred patch). (b) Three layers of edge nodes in normal direction to the edges, two layers of edge nodes in tangential direction to the edges.



Nonlinear PDEs with higher-order and/or mixed derivatives may require patches with more edge node layers as depicted in Figure 5b. The total number of edge nodes depends on the number of layers of the edge nodes. Our subsequent articles explore such staggered patch grids with more edge node layers for nonlinear wave PDEs, specifically for the viscous shallow water PDEs of Roberts and Li (2006) and the turbulent shallow water PDEs of Cao and Roberts (2016).

4 Multiscale staggered patch grid for weakly damped linear waves

This section shows that all the 60 centred multiscale staggered patch grids (defined in Section 3.2) give stable and accurate patch schemes for weakly damped linear wave PDEs (8) including the ideal waves with $c_D = c_V = 0$. This section focuses on the *spectral* patch scheme over 2D staggered

patch grids for a representative set of physical parameters c_D , c_V , and discretisation parameters n , δ , and Δ . A subsequent article will establish the stability, accuracy and sensitivity of several patch coupling schemes for a wide range of parameters.

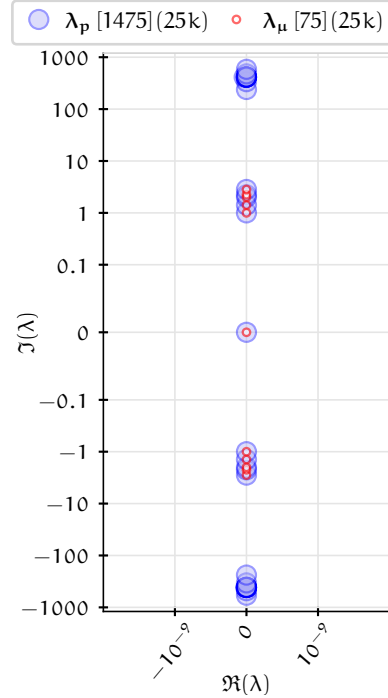
[Section 4.2](#) studies the dependence of the patch scheme stability on the patch grid geometry, the *geometry-stability study*, for all the 167 040 compatible 2D staggered patch grids (defined in [Section 3.2](#)). The geometry-stability study of [Section 4.2](#) shows that among all the compatible 167 040 compatible patch grids, only 1248 patch grids (0.75%) are stable—they all have symmetric patches. Based on some examples of unstable staggered patch grids, [Section 4.2](#) also shows that the more non-centred patches in a staggered patch grid, the more unstable modes in the patch scheme.

[Section 4.3](#) shows that none of the non-centred patch grids that are stable ([Section 4.2](#)) is accurate. Thus, among all the possible 167 040 compatible 2D staggered patch grids, only 120 centred patch grids (0.07%) are both stable and accurate.

Recall the patches are distributed on a macroscale spatial grid that is translationally invariant to macroscale shifts by multiples of 2Δ . Hence the macroscale, small wavenumber, modes of the patch scheme have a purely sinusoidal spatial structure—*exactly the same* sinusoidal spatial structure as that of the small wavenumber modes of the underlying microscale discrete model (3). Hence, in this scenario, the only error of the *macroscale* waves in the patch scheme is in their time dependence, which is completely characterised by their eigenvalues. Consequently, we establish the stability and accuracy of the patch scheme by comparing its *macroscale* eigenvalues with the corresponding eigenvalues of the full-domain microscale discretisation (3) for weakly damped linear waves PDEs (8). [Section 4.1](#) explains the method of deriving eigenvalues of a multiscale patch scheme (5) on a staggered patch grid.

For a first example, [Figure 6](#) shows the eigenvalues of the spectral patch scheme ([Section 4.1](#)) over the multiscale staggered patch grid #79985 of [Figure 3a](#) applied to the non-dissipative ideal waves (5) (when “+...” are omitted). As in [Figure 6](#), all the eigenvalue plots in this article have a legend that within brackets, $[\cdot]$, give the total number of eigenvalues for each set. Also, the legends give the total number of wavenumbers that each set of eigenvalues corresponds to within parentheses, $(\cdot k)$; the k here denotes the wavenumber k , not thousands. That the eigenvalues λ_p are all pure imaginary shows that the patch grid preserves the wave nature of the underlying microscale model, without introducing any significant artificial dissipation. The slow macroscale eigenvalues of the patch scheme ($|\Im(\lambda_p)| < 10$) agree to graphical accuracy with the corresponding slow eigenvalues λ_μ

Figure 6: Eigenvalues for non-dissipative ideal wave PDEs (8) with $c_D = c_V = 0$, over a $2\pi \times 2\pi$ periodic domain. Eigenvalues λ_p are for the spectral patch scheme (5) over the centred staggered patch grid #79985 (Figure 3a) with $N = 10$, $n = 6$, $r = 0.01$. Eigenvalues λ_μ are for the staggered full-domain microscale model (3). The microgrid interval $\delta = 2\pi/3000$ for both. The pure imaginary eigenvalues λ_p show that our patch scheme preserves the wave nature of the underlying system. The slow macroscale eigenvalues of the patch scheme ($|\Im(\lambda_p)| < 10$) agree to graphical accuracy with the corresponding slow eigenvalues λ_μ of the full-domain microscale model.



of the full-domain microscale model (3). Table 1 of Section 4.3 shows this agreement is exact (within 10^{-12}). This agreement implies that the slow macroscale dynamics on this staggered patch grid in Figure 3a accurately model the corresponding slow macroscale dynamics of the underlying microscale model.

As in Figure 6, all the eigenvalue plots in this article are on a quasi-log nonlinear scale using the arcsinh function. Specifically, we plot eigenvalues λ as points on the complex plane with real part $\text{arcsinh}(10^6 \cdot \Re\lambda)$ and complex part $\text{arcsinh}(100 \cdot \Im\lambda)$. This nonlinear arcsinh scale empowers us to see very small as well as very large values all together in the same plot, but unlike a log scale, for both positive and negative values.

4.1 Derive eigenvalues of a multiscale staggered patch scheme for linear microscale models

The method of deriving patch scheme eigenvalues in this subsection is applicable for linear wave-like PDEs over any of the 167 040 compatible 2D staggered patch grids, irrespective of the number of edge node layers in the patch scheme (Section 4). But the details of the discussions are for the specific staggered patch grid #79985 of Figure 5a with two layers of edge nodes in the normal direction to the edges, no edge nodes in the tangential

direction to the edges.

First, to compute the eigenvalues of the staggered microscale model (3) over the full-domain, we follow well established analysis (e.g., Hinch 2020, pp.138–139; Griffiths and Schiesser 2011)—which we summarise here to compare its results with the patch scheme. We substitute into the staggered finite difference system (3) an arbitrary Fourier mode² $h, u, v \propto \exp[i(k_x i\delta + k_y j\delta) + \lambda t]$ with real wavenumber (k_x, k_y) and complex growth rate λ . Then factoring the complex exponentials leads to the eigensystem

$$\mathbf{J}_\mu \begin{bmatrix} h \\ u \\ v \end{bmatrix} = \lambda_\mu \begin{bmatrix} h \\ u \\ v \end{bmatrix}, \quad (9)$$

where the subscript μ denotes the full-domain microscale staggered model (to distinguish it from the patch scheme), and where the Jacobian

$$\mathbf{J}_\mu := \begin{bmatrix} 0 & -i \sin(k_x \delta)/\delta & -i \sin(k_y \delta)/\delta \\ -i \sin(k_x \delta)/\delta & -c_D - c_V \omega_{\mu 0}^2 & 0 \\ -i \sin(k_y \delta)/\delta & 0 & -c_D - c_V \omega_{\mu 0}^2 \end{bmatrix},$$

with frequency $\omega_{\mu 0} := \sqrt{\sin^2(k_x \delta)/\delta^2 + \sin^2(k_y \delta)/\delta^2}$ corresponding to ideal waves ($c_D = c_V = 0$), for the staggered grid microscale model. For each wavenumber (k_x, k_y) , the three eigenvalues of the 3×3 Jacobian \mathbf{J}_μ are (one real and a complex conjugate pair),

$$\lambda_\mu = \begin{cases} -c_D + c_V \omega_{\mu 0}^2, \\ -(c_D + c_V \omega_{\mu 0}^2)/2 \pm i \sqrt{\omega_{\mu 0}^2 - [(c_D + c_V \omega_{\mu 0}^2)/2]^2}. \end{cases} \quad (10)$$

We assess the accuracy of a staggered patch scheme by comparing the eigenvalues of its macroscale modes (corresponding to small wavenumbers) with these eigenvalues (10) for the corresponding small wavenumber modes in the full-domain microscale model.

Second, we compute the eigenvalues of the staggered patch scheme (5). The dynamics of a staggered patch scheme reflects the coupled dynamics at two different length scales. One length scale is due to the microscale interactions within the patches, and the other length scale is due to the macroscale patch coupling. Hence, for eigenvalue analysis of a staggered patch scheme, the general mode needs to include spatial structures of the two scales: microscale within a patch, and macroscale across the patches.

²Throughout this article, i denotes the micro-grid index in x -direction, whereas $i := \sqrt{-1}$ is the imaginary unit.

- The staggered patch scheme (5) is invariant to translations in space by multiples of the macroscale spacing 2Δ . Hence the macroscale spatial structure can be expressed by complex exponential factors $\exp[i(k_x I\Delta + k_y J\Delta)]$. The indices I, J increment by multiples of two due to the translation symmetry.
- But the microscale spatial structure within the patches is not translationally invariant on the microscale: for example, nodes near a patch edge are different to nodes on the patch interior. Hence, in contrast to the full-domain microscale Fourier mode $h, u, v \propto \exp[i(k_x i\delta + k_y j\delta) + \lambda t]$, with constant amplitudes for h, u, v , a staggered patch scheme mode must allow for a general microscale spatial structure within the patches. We represent such sub-patch microscale structure by the variation with the sub-patch micro-grid indices i, j of the fields $h_{i,j}^{p,q}, u_{i,j}^{p,q}, v_{i,j}^{p,q}$ for each patch within a macro-cell (orange squares in Figure 4b); here $p, q \in \{0, 1\}$ is the local sub-macro-cell patch index.

Thus, for the eigenvalue analysis of a staggered patch scheme, we consider an arbitrary staggered patch scheme Fourier mode with real *macroscale wavenumber* (k_x, k_y) , over an infinite staggered grid of patches ($N \rightarrow \infty$ in Figure 5a),

$$\bullet h_{i,j}^{I,J}(t) = h_{i,j}^{p,q}(t) \exp[i(k_x I\Delta + k_y J\Delta)], \quad (11a)$$

$$\bullet u_{i,j}^{I,J}(t) = u_{i,j}^{p,q}(t) \exp[i(k_x I\Delta + k_y J\Delta)], \quad (11b)$$

$$\bullet v_{i,j}^{I,J}(t) = v_{i,j}^{p,q}(t) \exp[i(k_x I\Delta + k_y J\Delta)], \quad (11c)$$

for the sub-patch micro-grid indices (i, j) , global macroscale patch indices (I, J) , and local sub-macro-cell patch index (p, q) in the patch scheme (5). The local sub-cell patch indices, $p := I \bmod 2$ and $q := J \bmod 2$. Figure 4 illustrates these indices for an example case. In a finite space domain the global macroscale patch index $I, J \in \{0, 1, \dots, N-1\}$. For algebraic eigenvalue analysis, we invoke an infinite domain, $N \rightarrow \infty$, for which the macroscale patch index $I, J \in \mathbb{Z}$, the integers.

A staggered patch grid over the $2\pi \times 2\pi$ domain ($L = 2\pi$) with inter-patch distance Δ , resolves macroscale wavenumbers ranging from the smallest resolved wavenumber $k_x = k_y = 2\pi/L = 1$ to the largest resolved wavenumber $\lfloor 2\pi/(4\Delta) \rfloor = \lfloor \pi/(2\Delta) \rfloor$. Macroscale modes corresponding to these relatively small macroscale wavenumbers $|k_x|, |k_y| \leq \pi/(2\Delta)$ are all linearly independent on the macroscale patch grid, but not so for higher wavenumbers. Linear combinations of these linearly independent modes give general solutions to the patch systems (5), so we restrict the modes to this wavenumber range.

In the patch scheme mode (11), the time-dependent microscale spatial structure $h_{i,j}^{p,q}(t)$, $u_{i,j}^{p,q}(t)$, $v_{i,j}^{p,q}(t)$ is *spatially modulated* by the macroscale wave form $\exp[i(k_x I\Delta + k_y J\Delta)]$. The microscale structure $h_{i,j}^{p,q}(t)$, $u_{i,j}^{p,q}(t)$, $v_{i,j}^{p,q}(t)$ depends on the sub-macro-cell patch index p, q and the sub-patch micro-grid node index i, j , but not on the global patch index I, J .

In eigenvalue analysis of a patch scheme, the time-dependent microscale structure $h_{i,j}^{p,q}(t)$, $u_{i,j}^{p,q}(t)$, $v_{i,j}^{p,q}(t)$ in the patch scheme Fourier mode (11) corresponds to the interior nodes of all patches in any one macro-cell, indicated by the orange square in Figure 5a. Collecting the interior values of all patches in the macro-cell into a vector gives the *state vector* x^i ; the superscript $(\cdot)^i$ is not an index or exponent, instead, a qualifier denoting the patch interior nodes of one macro-cell (we use $(\cdot)^I$ to denote the interior nodes of all the macro-cells in the full system (7)). For the example patch grid #79985 of Figures 3a and 5, the total number of patch interior nodes per macro-cell, that is the size of x^i ,

$$n_p^i = 9n^2/4 - 4n + 2, \quad (12)$$

where n is the number of sub-patch micro-grid intervals. For example, for the cases of $n = 6, 10, 14$ sub-patch micro-grid intervals, $n_p^i = 59, 187, 387$ respectively. For the specific staggered patch grid #79985 with $n = 6$ sub-patch micro-grid intervals, the state vector containing 59 elements is

$$\begin{aligned} x^i = & (h_{1,1}^{0,0}, h_{1,3}^{0,0}, h_{1,5}^{0,0}, h_{3,1}^{0,0}, h_{3,3}^{0,0}, h_{3,5}^{0,0}, h_{5,1}^{0,0}, h_{5,3}^{0,0}, h_{5,5}^{0,0}, u_{2,1}^{0,0}, u_{2,3}^{0,0}, \\ & u_{2,5}^{0,0}, u_{4,1}^{0,0}, u_{4,3}^{0,0}, u_{4,5}^{0,0}, v_{1,2}^{0,0}, v_{1,4}^{0,0}, v_{3,2}^{0,0}, v_{3,4}^{0,0}, v_{5,2}^{0,0}, v_{5,4}^{0,0}, h_{1,2}^{0,1}, h_{1,4}^{0,1}, \\ & h_{3,2}^{0,1}, h_{3,4}^{0,1}, h_{5,2}^{0,1}, h_{5,4}^{0,1}, u_{2,2}^{0,1}, u_{2,4}^{0,1}, u_{4,2}^{0,1}, u_{4,4}^{0,1}, v_{1,1}^{0,1}, v_{1,3}^{0,1}, v_{3,1}^{0,1}, v_{3,3}^{0,1}, \\ & v_{3,5}^{0,1}, v_{5,1}^{0,1}, v_{5,3}^{0,1}, v_{5,5}^{0,1}, h_{2,1}^{1,0}, h_{2,3}^{1,0}, h_{2,5}^{1,0}, h_{4,1}^{1,0}, h_{4,3}^{1,0}, h_{4,5}^{1,0}, u_{1,1}^{1,0}, \\ & u_{1,3}^{1,0}, u_{1,5}^{1,0}, u_{3,1}^{1,0}, u_{3,3}^{1,0}, u_{3,5}^{1,0}, u_{5,1}^{1,0}, u_{5,3}^{1,0}, u_{5,5}^{1,0}, v_{2,2}^{1,0}, v_{2,4}^{1,0}, v_{4,2}^{1,0}, v_{4,4}^{1,0}). \end{aligned} \quad (13)$$

Recall that the patch coupling (spectral throughout this article) gives the edge values of each patch as a function of the aggregate values of all the patches. Hence a patch coupling gives edge values of all the patches in a macro-cell in terms of the substituted macroscale mode wavenumber. Collecting the edge values of all patches in the macro-cell into a vector gives the *edge vector* x^e ; the superscript $(\cdot)^e$ is not an index or exponent, instead, a qualifier denoting the edge nodes of one macro-cell (we use E to denote the edge nodes of all the macro-cells in the full system (7)). For the particular staggered patch grid #79985 in Figure 5a, the total number of patch edge nodes per macro-cell for weakly damped linear wave, that is the size of the edge vector x^e , is $n_p^e = 18n - 16$, where n is the number of sub-patch micro-grid intervals: for $n = 6, 10, 14$, the vector size $n_p^e = 92, 164, 236$, respectively. This n_e^i is only for the 48 centred patch grids with three

patches per macro-cell (Figure 5a), the 72 centred patch grids with four patches per macro-cell have more edge nodes.

Substituting the macroscale Fourier mode (11), and the coupled patch edge values computed by the patch coupling, into the staggered patch scheme (5) of the wave PDEs (8) gives the time evolution of a staggered patch scheme as a linear dynamical system

$$\frac{d\mathbf{x}^i}{dt} = \mathbf{F}(\mathbf{x}^i; \mathbf{x}^e(\mathbf{x}^i)) = \mathbf{J}_p \mathbf{x}^i, \quad (14)$$

where the Jacobian $\mathbf{J}_p := \partial \mathbf{F} / \partial \mathbf{x}^i$. This system is parametrised by the macroscale wavenumber (k_x, k_y) . There are n_p^i variables corresponding to each macroscale wavenumber (k_x, k_y) . The state vector \mathbf{x}^i of the full-size staggered patch scheme dynamical system (7) contain interior values of all the patches in a staggered patch grid, but the state vector \mathbf{x}^i of the staggered patch scheme dynamical system (14) for one macroscale wave-number (k_x, k_y) contain interior values of only one macro-cell. Hence, we call equation (14) the *one-cell system* of a staggered patch scheme. Similarly, we call the Jacobian \mathbf{J}_p as the *one-cell Jacobian* of a staggered patch scheme.

The $n_p^i \times n_p^i$ one-cell Jacobian \mathbf{J}_p depends on the physical parameters c_D and c_V , discretisation parameters n , δ , and Δ , and the macroscale wave-number (k_x, k_y) . For the example patch grid #79985 in Figure 5a, for $n = 6$ sub-patch micro-grid intervals, the one-cell Jacobian \mathbf{J}_p is a 59×59 sparse matrix with at most only 318 nonzero elements of its 3481 elements. Such sparsity holds irrespective of the particular patch coupling interpolation.

By considering all macroscale wavenumbers (k_x, k_y) , the one-cell Jacobian \mathbf{J}_p provides a complete general solution for every initial condition applied to a given patch scheme. Let the eigenvalues and eigenvectors of \mathbf{J}_p be denoted by λ_l and \mathbf{e}_l respectively. Then by the linearity of (14), a general solution is a linear combination of the set of $\mathbf{e}_l \exp(\lambda_l t)$. So stability is assured if the eigenvalues $\{\lambda_l\}$ all have nonpositive real parts. The few eigenvectors \mathbf{e}_l that have spatial structures that are slowly varying within the patches are the macroscale modes in the patch scheme. It is the eigenvalues of these modes that we compare for accuracy with the small wavenumber eigenvalues of the full-domain system. The other eigenvectors \mathbf{e}_l , those with significant sub-patch structure, are micro-scale modes modulated over a macroscale. They are not physically significant, and so we do not compare their eigenvalues with that of the underlying full-domain system, although we do require that they be stable. It is in this way that the eigenvalues of the Jacobian \mathbf{J}_p characterise the stability and accuracy of a given patch scheme.

We attempted to derive algebraic expressions for the eigenvalues of a one-cell Jacobian \mathbf{J}_p , through various algebraic simplification strategies, in the three Computer Algebra Systems (CAS) SymPy, Reduce, and Maple. For general macroscale wavenumber (k_x, k_y) , the three CAS packages failed to compute (no results in 48 hours) the analytic eigenvalues of the 59×59 Jacobian ($n = 6$). That is, unlike the expression (10) for the full-domain microscale models, expressing the eigenvalues algebraically appears infeasible for the patch scheme. Hence, we compute the patch scheme eigenvalues λ_p by numerically evaluating the one-cell Jacobian for a range of values of the macroscale wavenumber (k_x, k_y) , physical parameters c_D and c_V , and discretisation parameters n , δ , and Δ .

Sections 4.2 and 4.3 assess the staggered patch grids by comparing eigenvalues λ_p of a patch scheme one-cell Jacobian \mathbf{J}_p with the eigenvalues λ_μ of the full domain microscale model, for all the macroscale wavenumbers (k_x, k_y) resolved by a finite macroscale staggered grid.

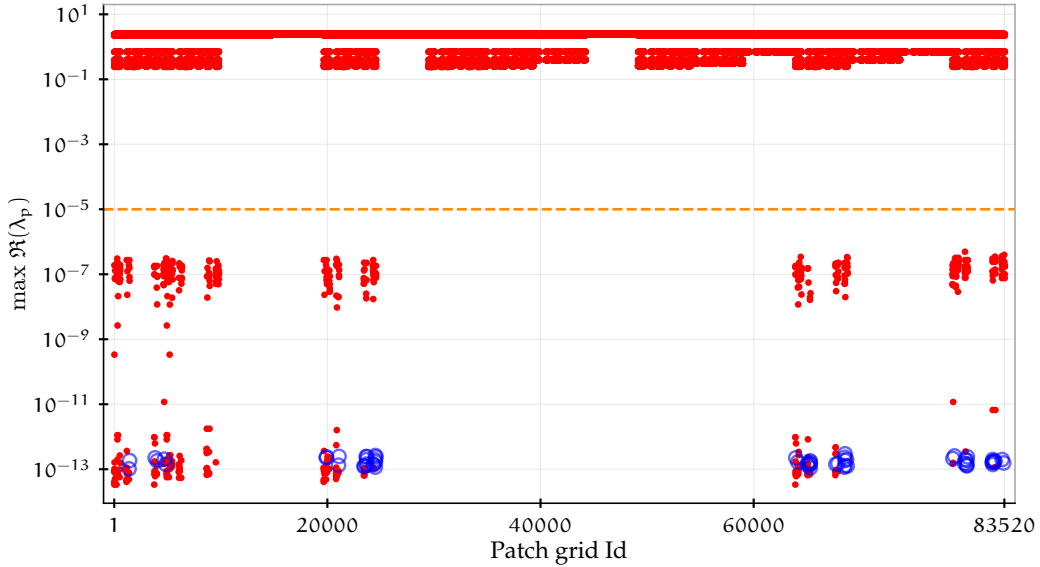
4.2 Only patch grids with all symmetric patches are stable

Section 3.2 introduces compatible multiscale staggered patch grids for wave-like systems and shows that there are 167 040 such compatible 2D patch grids. Among these staggered patch grids, 120 of them are *centred staggered patch grids* (e.g., the two patch grids in Figure 3) whose sub-patch micro-grids all have a centre node and include a centred-patch corresponding to each of the state variables. That is, the centred patch grids consist of each of the green highlighted patches in Figure 2 and the fourth patch may also be one such centred patch or an empty patch. The remaining 166 920 are *non-centred staggered patch grids*. This subsection studies the dependence of the patch scheme stability on the patch grid geometry, the *geometry-stability study*, for all these 167 040 compatible 2D patch grids for the weakly damped linear wave PDEs (8).

We define a *staggered patch scheme to be stable* when the maximum real part of its *numerically computed* eigenvalues $\max \Re(\lambda_p) < 10^{-5}$ (to allow for tiny round-off errors). And herein we define a *staggered patch grid to be stable* if the spectral staggered patch scheme is stable over that grid.

We analyse the stability of all the 167 040 staggered patch grids separately for two groups based on the number of sub-patch micro-grid intervals n . First, we analyse the 83 520 patch grids with odd $n/2$, taking $n = 6$ as a representative case; second the 83 520 patch grids with even $n/2$, taking $n = 4$ as a representative case. Figure 7 plots the maximum real parts of the spectral patch scheme eigenvalues $\max \Re(\lambda_p)$ over all 83 520 compatible

Figure 7: Maximum real parts of the spectral patch scheme eigenvalues $\max \Re(\lambda_p)$ over all 83 520 compatible 2D staggered patch grids with $N = 10$, $n = 6$, $r = 0.1$ for ideal wave PDEs (8) with $c_D = c_V = 0$. Among the non-centred patch grids (red dots), 82 896 are unstable ($\max \Re(\lambda_p) > 10^{-5}$), 564 are stable ($\max \Re(\lambda_p) < 10^{-5}$). All 60 centred staggered patch grids (blue circles) are stable.



2D staggered patch grids with $N = 10$, $n = 6$, $r = 0.1$ for ideal wave PDEs (8) with $c_D = c_V = 0$. The red dots are for non-centred patch grids, and the blue circles are for centred patch grids. In each patch grid, each of the four patches in a macro-cell is chosen from any of the 16 micro-grids in Figure 2b or an empty patch, excluding the all-empty patch. Hence, Figure 7 is representative of the staggered patch grids with odd $n/2$. In Figure 7, among the non-centred patch grids (red dots), only 564 of them are stable according to $\max \Re(\lambda_p) < 10^{-5}$, all the remaining 82 896 of the non-centred patch grids are unstable with $\max \Re(\lambda_p) > 10^{-5}$. That is, 99.32% of the non-centred patch grids are unstable. On the other hand all 60 of the centred staggered patch grids (blue circles) are stable with $\max \Re(\lambda_p) < 3 \cdot 10^{-13}$. That is, *almost all non-centred patch grids lead to unstable patch schemes but all centred patch grids constitute stable patch schemes.*

In Figure 7, all 564 stable non-centred patch grids (red dots with $\max \Re(\lambda_p) < 10^{-5}$), contain only symmetric patches $uuvv$, $hhvv$, $uuhh$, and $hhhh$ from Figure 2b or an empty patch. All 60 stable centred patch grids (blue circles with $\max \Re(\lambda_p) < 3 \cdot 10^{-13}$), contain only h -, u -, and v -centred patches from Figure 2b or an empty patch, which are also symmetric patches. Thus,

Figure 7 shows that among all 83 520 staggered patch grids, *only patch grids containing symmetric patches are stable*. On the other hand, only $5^4 - 1 = 624$ staggered patch grids are possible using only the symmetric patches $uuvv$, $hhvv$, $uuhh$, and $hhhh$ from Figure 2b or an empty patch, excluding the all-empty patch. Among these 60 are centred patch grids and the remaining 564 are non-centred patch grids. Figure 7 shows all these 624 patch grids with symmetric patches are stable. This shows that *all patch grids containing only symmetric patches are stable*. That is, *using only symmetric patches is a necessary and sufficient condition for patch scheme stability*.

As a representative of the staggered patch grids with even $n/2$, since even cases are potentially different to the odd cases, we plotted the maximum real parts of the eigenvalues for $n = 4$ (not included). The plot was qualitatively the same as Figure 7 except that the clusters of stable patch grids occur around different patch grid Ids than in Figure 7. Such a difference is because the centredness depends upon whether $n/2$ is odd or even (green highlighted names in Figures 2a and 2b). For $n = 4$, the spectral patch is stable, $\max \Re(\lambda_p) < 10^{-5}$, for all the 624 staggered patch grids that contain only symmetric patches $uuvv$, $hhvv$, $uuhh$, and $hhhh$ from Figure 2a or an empty patch. That plot of $\max \Re(\lambda_p)$ for $n = 4$ also confirms the same two conclusions in the preceding two paragraphs, including the same number of stable and unstable patch grids. Thus, for both the cases of $n/2$ being odd or even, among all the possible 167 040 compatible 2D staggered patch grids, only $624 + 624 = 1248$ patch grids (0.75%) are stable.

Including the dissipation in the linear wave PDEs (8) by nonzero dissipation coefficients c_D, c_V stabilize the patch schemes by pushing the positive real parts of the eigenvalues to negative values. Hence all these 1248 patch grids are also stable for weakly damped linear waves.

This paragraph discusses three examples of unstable non-centred staggered patch grids and their eigenvalues. Firstly, Figure 8 shows the non-centred patch grid #55420 and the corresponding eigenvalues of the spectral patch scheme for discretisations of wave PDEs (8) with $c_D = c_V = 0$. The patch grid #55420 (Figure 8a) has the non-centred patch $uhvh$ (Figure 2b) in place of the h -patch of #79985 (Figure 3a). That one change to a non-centred patch makes the patch grid #55420 unstable with large real part eigenvalues $\max \Re(\lambda_p) = 0.3$ (Figure 8b). There are 80 unstable modes with $\max \Re(\lambda_p) > 10^{-5}$ in Figure 8b for the non-centred patch grid #55420. Secondly, replacing the u -patch with the non-centred patch $huvh$ (Figure 2b) in the patch grid #55420 of Figure 8a, gives the non-centred patch grid #56287 which we found has 176 unstable modes (plot not included). Lastly, replacing also the v -patch in #56287 with the non-centred patch $uhhv$ (Figure 2b) gives the patch grid #56236 in Figure 9a whose patches are all non-centred.

Figure 8: Non-centred staggered patch grid #55420 over which spectral patch scheme is unstable for ideal wave PDEs (8) with $c_D = c_V = 0$.

- (a) This non-centred patch grid #55420 has the non-centred patch uhvh from Figure 2b in place of the h-patch of the patch grid #79985 (Figure 3a); that is the only difference.
- (b) Eigenvalues of spectral patch scheme over patch grid #55420 has large positive real parts, $\max \Re(\lambda_p) = 0.3$.

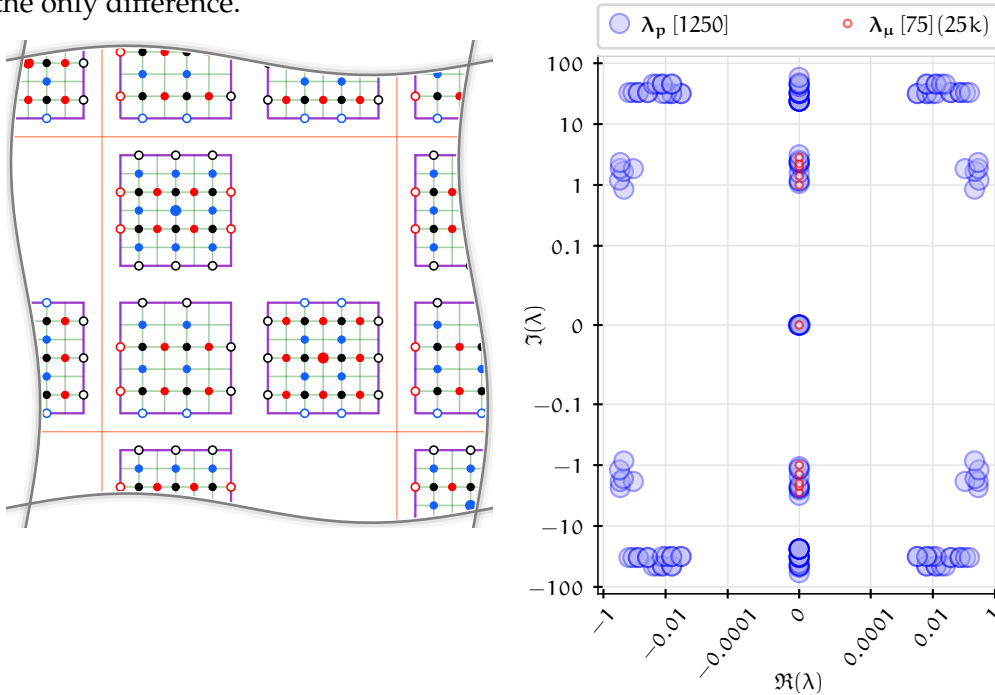


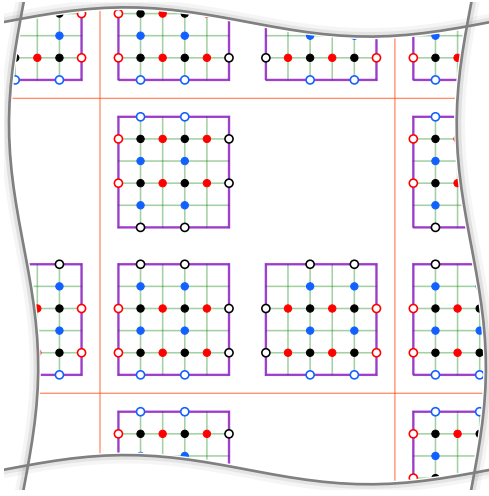
Figure 9b plots the eigenvalues for this non-centred patch grid #56236: it shows 272 unstable modes with $\max \Re(\lambda_p) > 10^{-5}$. It appears that the more non-centred patches in a staggered patch grid, the more modes are unstable.

4.3 Only centred patch grids are accurate

This subsection shows that all the 60 centred staggered patch grids give accurate patch schemes, but none of the stable non-centred patch grids in Figure 7 is accurate. We first discuss discretisations of the ideal wave PDEs (8) ($c_D = c_V = 0$), and second explore weakly damped linear waves with nonzero c_D, c_V . This subsection also illustrates several features and correlations in the structure of the eigenvalues of the patch scheme for weakly damped linear waves.

Figure 9: Non-centred patch grid #56236 leads to more unstable modes compared to patch grid #55420 of Figure 8a for ideal waves.

(a) Replacing h -, u -, v -patches of the centred patch grid #79985 (Figure 3a) with non-centred patches $uhvh$, $huvh$, $uhhv$ (Figure 2b) respectively, gives this non-centred patch grid #56236.



(b) Eigenvalues of spectral patch scheme over patch grid #56236 has large positive real parts, $\max \Re(\lambda_p) = 0.3$.

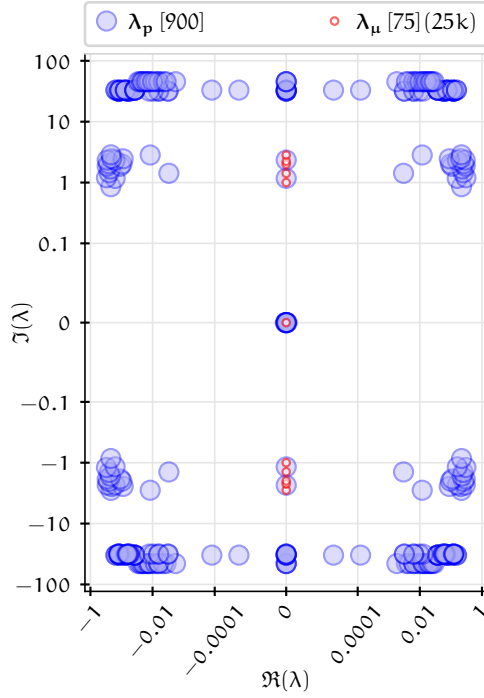


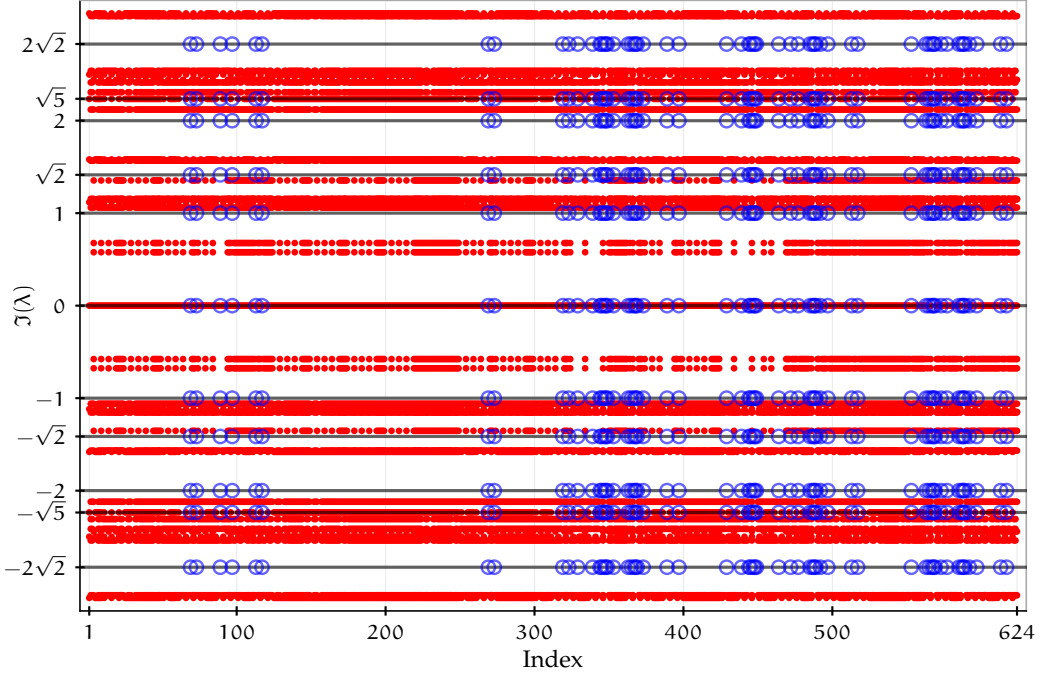
Table 1: Slow macroscale eigenvalues λ_p of the patch scheme (5), $|\Im(\lambda_p)| < 10$ in Figure 6, agree exactly (within 10^{-12}) with the corresponding eigenvalues λ_μ of the full-domain microscale model (3). All the distinct ideal wave frequencies $\omega_{\mu 0}$ (red circles in Figure 6) correspond to the resolved macroscale wavenumbers $k_x, k_y = 0, \pm 1, \pm 2$ on the patch grid #79985 with $N = 10$. Error $\epsilon_k = \max_i (|\lambda_{p,i} - \lambda_\mu|)$ for each wavenumber.

$\omega_{\mu 0}$	(k_x, k_y)	ϵ_k
-2.8284	(-2, -2)	$2.0 \cdot 10^{-13}$
-2.2361	(-2, -1)	$2.6 \cdot 10^{-13}$
-2.0000	(-2, 0)	$2.0 \cdot 10^{-13}$
-1.4142	(-1, -1)	$1.6 \cdot 10^{-13}$
-1.0000	(-1, 0)	$2.7 \cdot 10^{-13}$
0.0000	(0, 0)	$2.9 \cdot 10^{-14}$
1.0000	(1, 0)	$2.3 \cdot 10^{-13}$
1.4142	(1, 1)	$1.2 \cdot 10^{-13}$
2.0000	(2, 0)	$1.3 \cdot 10^{-13}$
2.2361	(2, 1)	$2.1 \cdot 10^{-13}$
2.8284	(2, 2)	$1.9 \cdot 10^{-13}$

This paragraph illustrates the accuracy of the centred staggered patch grid #79985 for ideal waves. For non-dissipative ideal wave PDEs (8) ($c_D = c_V = 0$), Figure 6 compares eigenvalues λ_p of the patch scheme (5) with eigenvalues λ_μ of the full-domain microscale model (3) with the same micro-grid interval $\delta = 2\pi/3000$. Figure 6 shows that the slow macroscale eigenvalues, $|\Im(\lambda_p)| < 10$, of the patch scheme agree to graphical accuracy with the eigenvalues λ_μ of the full-domain microscale staggered model. Table 1 shows this agreement is exact (within 10^{-12}). First column in Table 1 lists all the distinct ideal wave frequencies $\omega_{\mu 0} = \Im(\lambda_\mu)$ corresponding to the red circles in Figure 6, using the eigenvalue expression (10). The second column lists all the resolved macroscale wavenumbers $k_x, k_y = 0, \pm 1, \pm 2$ on the patch grid #79985 with $N = 10$ that corresponds to these $\omega_{\mu 0}$. For each of these wavenumbers, there are several repeated patch scheme eigenvalues λ_p (blue circles in Figure 6). For each of these wavenumbers, the third column lists the errors $\epsilon_k = \max_i (|\lambda_{p,i} - \lambda_\mu|)$ between the eigenvalues of the patch scheme and that of the full-domain model. The small overall maximum error of $\epsilon_k = 2.7 \cdot 10^{-13}$ (within numerical roundoff error) shows that slow macroscale eigenvalues λ_p and λ_μ agree exactly. That is, the centred staggered patch grid #79985 gives accurate multiscale spectral patch schemes for ideal waves.

This paragraph shows that all the centred staggered patch grids give accurate multiscale spectral patch schemes for ideal waves. The previous Section 4.2 shows that all 624 patch grids containing only symmetric patches are stable (i.e., in Figure 2b, patches $uuvv$, $hhvv$, $uuhh$, $hhhh$, or empty). The negligible $\max \Re(\lambda_p)$ of these stable schemes agrees with the zero real parts in the eigenvalue expression (10) for full-domain microscale model of ideal waves ($c_D = c_V = 0$). That all eigenvalues λ_p are pure imaginary (to numerical error) shows that the staggered patch grid preserves waves without introducing any significant artificial dissipation. Hence, to assess the accuracy of all those 624 stable staggered patch grids, it is sufficient to compare the imaginary parts of the eigenvalues. Figure 10 plots the imaginary parts of the slow macroscale eigenvalues, those for which $|\Im(\lambda_p)| < 10$, for all the 624 stable staggered patch grids that contain only symmetric patches. The horizontal black lines in Figure 10 correspond to the ideal wave frequencies $\omega_{\mu 0} = \Im(\lambda_\mu) = \sqrt{\sin^2(k_x \delta)/\delta^2 + \sin^2(k_y \delta)/\delta^2} \approx (0, \pm 1, \pm\sqrt{2}, 2, \pm\sqrt{5}, \pm 2\sqrt{2})$ from the eigenvalue expression (10) for macroscale wavenumbers $k_x, k_y = 0, \pm 1, \pm 2$ and $\delta = 2\pi/300$. For all 60 centred patch grids (blue circles) $\Im(\lambda_p)$ agree exactly with $\Im(\lambda_\mu)$ (black lines) of full-domain microscale model (3) (within numerical roundoff errors). On the other hand, for none of the 564 non-centred patch grids $\Im(\lambda_p)$ (red dots)

Figure 10: Imaginary parts of spectral patch scheme macroscale eigenvalues ($|\Im(\lambda_p)| < 10$) for all 624 stable staggered patch grids that contain only symmetric patches, with $N = 10$, $n = 6$, $r = 0.1$ for ideal wave PDEs (8) with $c_D = c_V = 0$. For all 60 centred patch grids $\Im(\lambda_p)$ (blue circles) agree with $\Im(\lambda_\mu)$ (black lines) of full-domain microscale model (3). For none of the 564 non-centred patch grids $\Im(\lambda_p)$ (red dots) agree with all the $\Im(\lambda_\mu)$.

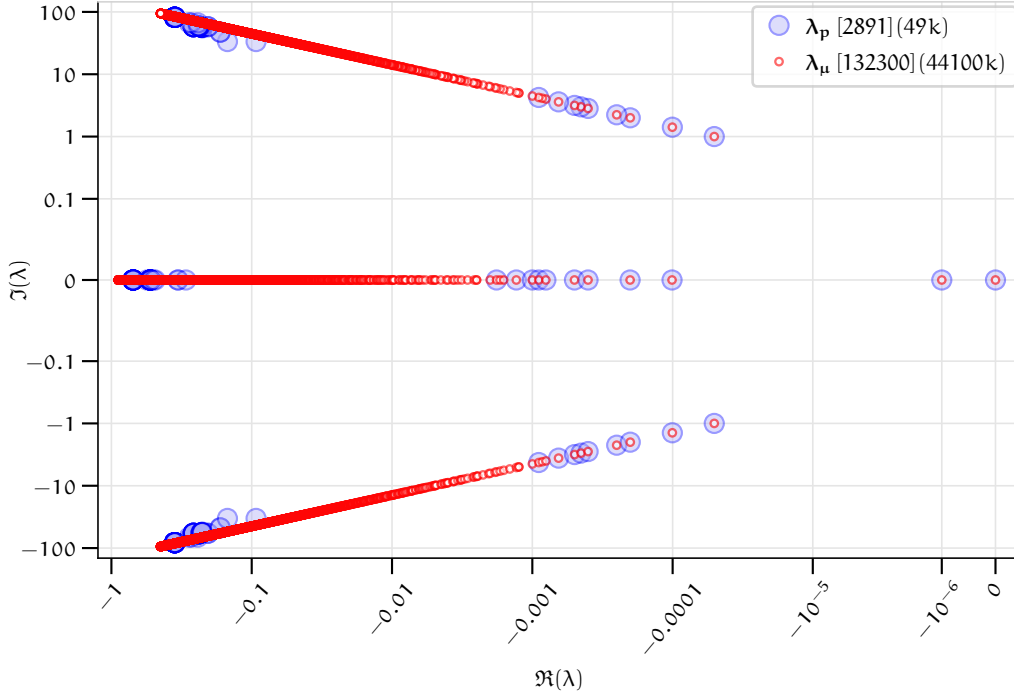


agree with all the $\Im(\lambda_\mu)$ (black lines). That is, *for ideal waves, all the 60 centred staggered patch grids give accurate patch schemes, but none of the stable non-centred patch grids is accurate.*

Several features in the structure of patch scheme eigenvalues become clearer when plotted for cases of the weakly damped linear wave PDEs (8) with nonzero dissipation coefficients c_D, c_V . The rest of this subsection discusses the structure of patch scheme eigenvalues and establishes the patch scheme accuracy for weakly damped linear wave PDEs (8). Unless otherwise noted, we show and discuss the case of small bed drag with $c_D = 10^{-6}$ and small viscous dissipation with $c_V = 0.0001$.

Figure 11 compares the patch scheme eigenvalues λ_p with the eigenvalues λ_μ of the full-domain microscale model (3) for the weakly damped linear wave. The eigenvalues λ_p in Figure 11 are for the spectral patch scheme over the centred staggered patch grid #79985 (Figure 3a) over a non-dimensional $2\pi \times 2\pi$ domain ($L = 2\pi$) with 14×14 ($N = 14$) macro-grid inter-

Figure 11: Eigenvalues for weakly damped linear waves ($c_D = 10^{-6}$, $c_V = 0.0001$) over a $2\pi \times 2\pi$ periodic domain with the micro-grid interval $\delta = 2\pi/420$. For macroscale modes with $\Re(\lambda) > -0.01$ and $|\Im(\lambda)| < 10$, the eigenvalues λ_p of the spectral staggered patch scheme ($N = 14$, $n = 6$, $r = 0.1$) agree exactly with eigenvalues λ_μ of the staggered full-domain microscale model.



vals, 6×6 ($n = 6$) sub-patch micro-grid intervals, and patch scale ratio $r = 0.1$. Hence, the macro-grid interval $\Delta = L/N = 2\pi/14$ (violet macro-grid) and the sub-patch micro-grid interval $\delta = l/n = 2Lr/(Nn) = 2\pi/420 \approx 0.015$ (green sub-patch micro-grid). A staggered patch grid with $N = 14$ macro-grid intervals resolves $N^2/4 = 49$ macroscale wavenumbers (k_x, k_y) which is same as the number of macro-cells. As per the count (12), such a staggered patch grid has $n_p^i = 9n^2/4 - 4n + 2 = 59$ patch interior nodes per macro-cell forming the one-cell state vector \mathbf{x}^i in the expression (13). Hence, for each macroscale wavenumber (k_x, k_y) resolved by the staggered patch grid, the $n_p^i \times n_p^i$ one-cell Jacobian \mathbf{J}_p in the linear system (14) gives $n_p^i = 59$ eigenvalues λ_p . Numerically evaluating \mathbf{J}_p for all 49 macroscale wavenumbers (k_x, k_y) then gives $49 \cdot 59 = 2891$ patch scheme eigenvalues λ_p . As required, this matches the total number of patch interior nodes n_p^i (the number of state variables) from the expression (6) for this case of $N = 14$

and $n = 6$.

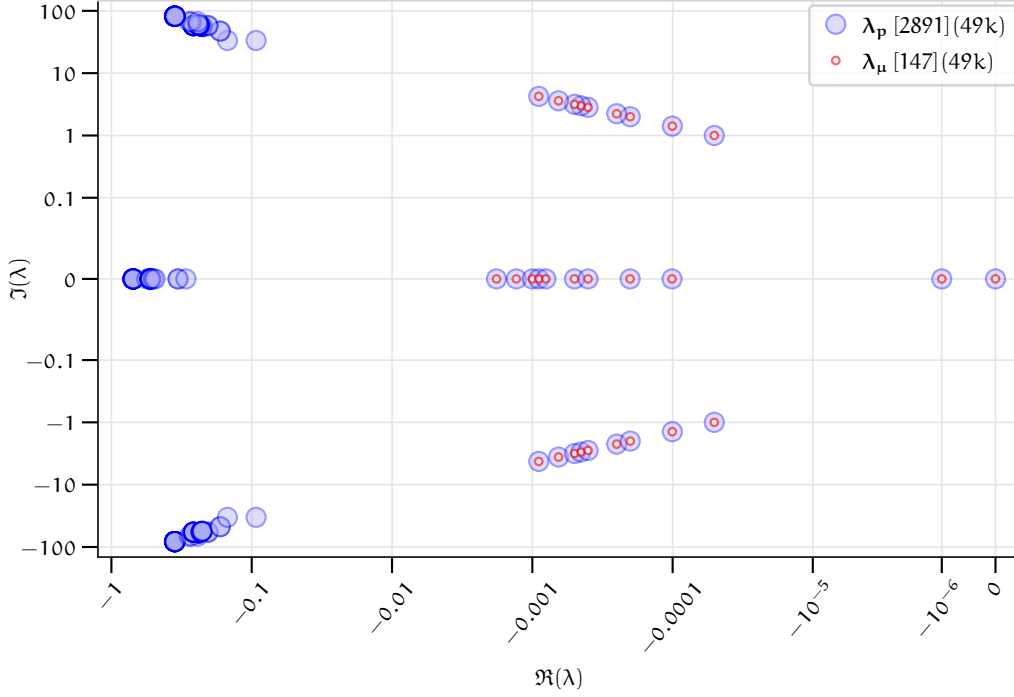
The staggered full-domain microscale model for [Figure 11](#) is over the full-domain micro-grid ([Figure 1](#), right) whose micro-grid interval is of the same size as the sub-patch micro-grid interval $\delta = 2\pi/420$ of the patch scheme for the figure. Such a full-domain micro-grid has $n = L/\delta = 420$ micro-grid intervals and resolves $n^2/4 = 44\,100$ wavenumbers (k_x, k_y) . For each wavenumber (k_x, k_y) resolved on the staggered full-domain micro-grid, the 3×3 Jacobian \mathbf{J}_μ in the linear system (9) gives 3 eigenvalues λ_μ , as in the expression (10). Thus, evaluating the expression (10) for all the 44 100 wavenumbers gives $44\,100 \cdot 3 = 132\,300$ full-domain microscale eigenvalues λ_μ . As required, this matches the total number of full-domain microscale nodes $3n^2/4$ (the number of state variables) for $n = 420$ ([Section 2](#)).

In [Figure 11](#), the eigenvalues λ_μ of the staggered full-domain microscale model (small red circles) denote the modes corresponding to all 44 100 resolved wavenumbers, *ranging uniformly across the spatial scales*, from the smallest resolved wavenumber $k_x = k_y = 2\pi/L = 1$ to the largest resolved wavenumber $2\pi/(4\delta) = 105$. On the other hand, the eigenvalues λ_p of the multiscale staggered patch scheme (large blue circles) correspond to two qualitatively different modes at two different spatial scales, pure *macroscale modes* and *sub-patch microscale modes*, with a gap between their spatial scales. This gap in the spatial scales also leads to a gap in their time scales, evident in the *spectral gap* where there are no patch scheme eigenvalues roughly between $-0.1 \lesssim \Re(\lambda_p) \lesssim -0.001$ in [Figure 11](#).

- *Macroscale modes* are those patch scheme modes (eigenvectors) that have macroscale structure (spatial variation) with little microscale structure. The eigenvalues corresponding to these macroscale modes are *macroscale eigenvalues* ($\Re(\lambda_p) \gtrsim -0.001$ in [Figure 11](#)).
- *Microscale modes* are those patch schemes modes that have significant microscale structure irrespective of whether it is modulated by some macroscale structure. The eigenvalues corresponding to these microscale modes are *microscale eigenvalues* ($\Re(\lambda_p) \lesssim -0.1$ in [Figure 11](#)).

Plots (omitted in this article) of corresponding eigenvectors confirm the above division into macroscale and microscale modes ([Divahar 2022, §3.2.6](#)). The macroscale eigenvalues λ_p on the right five clusters correspond to all the $N^2/4 = 49$ macroscale wavenumbers resolved by the staggered patch grid, ranging from the smallest macroscale wavenumber $k_x = k_y = 2\pi/L = 1$ to the largest resolved wavenumber $\lfloor 2\pi/(4\Delta) \rfloor = \lfloor N/4 \rfloor = 3$; that is the macroscale wavenumber $k_x, k_y \in \{-3, -2, -1, 0, 1, 2, 3\}$. The

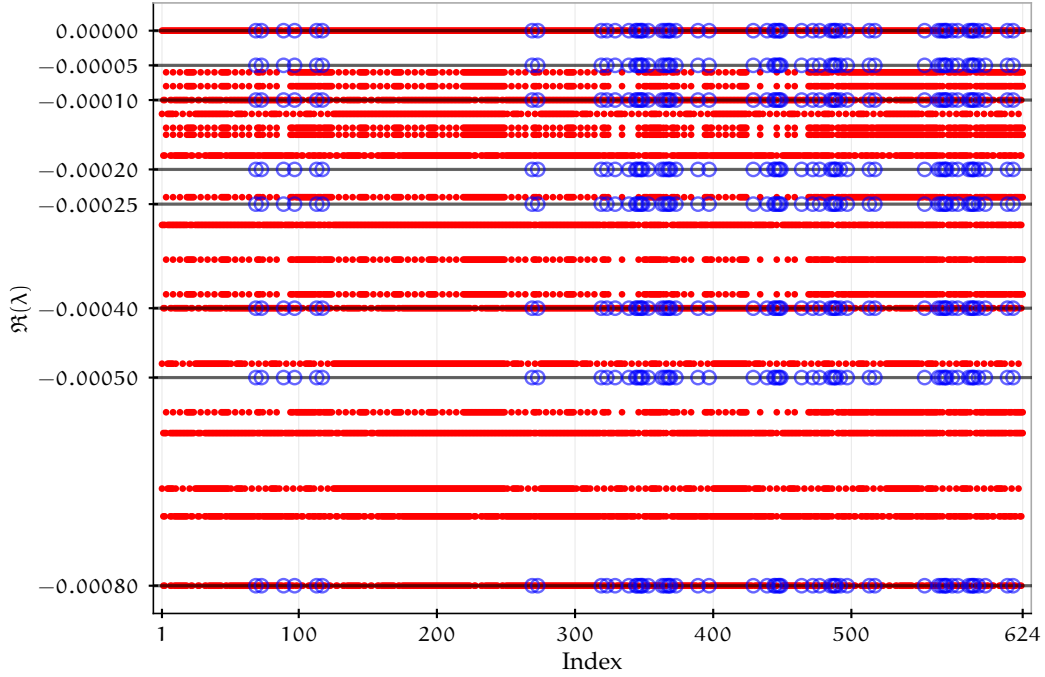
Figure 12: *All* macroscale eigenvalues λ_p agree exactly with eigenvalues λ_μ . Same as Figure 11 except here the eigenvalues λ_μ of staggered full-domain microscale model are plotted only for those $N^2/4 = 49$ macroscale wavenumbers resolved by the staggered patch grid.



microscale eigenvalues λ_p on the left three clusters correspond to sub-patch microscale modes modulated over the macroscale, whose modulated wavenumbers range from the smallest sub-patch microscale wavenumber $k_x = k_y = 2\pi/l = 2\pi/(2rL/N) = 70$ to the largest sub-patch microscale wavenumber $2\pi/(4\delta) = 105$. Hence, the gap between the largest resolved macroscale wavenumber and the smallest sub-patch microscale wavenumber spanning $(\lfloor N/4 \rfloor, 2\pi/(2rL/N)) = (3, 70)$, is the gap in spatial scales that a patch scheme does not resolve. In Figure 11, the *spectral gap* where there are no patch scheme eigenvalues roughly between $-0.1 \lesssim \Re(\lambda_p) \lesssim -0.001$, corresponds to these spatial scales unresolved by the patch scheme.

Figure 12 plots the eigenvalues λ_μ corresponding to only those $N^2/4$ macroscale wavenumbers resolved by the staggered patch grid. Similar to Figure 6 for ideal wave, Figure 12 for weakly damped linear wave clearly shows that *all* macroscale eigenvalues λ_p with $\Re(\lambda_p) > -0.01$ and $|\Im(\lambda_p)| < 10$ agree exactly (within numerical roundoff errors) with eigenvalues λ_μ of

Figure 13: Real parts of spectral patch scheme macroscale eigenvalues ($\Re(\lambda_p) > -0.01$ and $|\Im(\lambda_p)| < 10$) for all 624 stable staggered patch grids that contain only symmetric patches, with $N = 10$, $n = 6$, $r = 0.1$ for weakly damped linear wave PDEs (8) with $c_D = 10^{-6}$, $c_V = 0.0001$. For all 60 centred patch grids $\Re(\lambda_p)$ (blue circles) agree with $\Re(\lambda_\mu)$ (black lines) of full-domain microscale model (3). For none of the 564 non-centred patch grids $\Re(\lambda_p)$ (red dots) agree with all the $\Re(\lambda_\mu)$.



the full-domain microscale model for the same macroscale wavenumbers. That is, the equation-free multiscale spectral patch scheme on the staggered patch grid #79985 (Figure 5a) accurately resolves the macroscale weakly damped linear waves.

As Section 2 discusses, it is the microscale computational model that a multiscale patch scheme seeks to predict accurately, not directly the PDE model. That is, how well the full-domain microscale models (2) and (3) predict the solutions of the PDEs (1) is a peripheral issue.

Centred staggered patch grids give accurate multiscale spectral patch scheme for weakly damped linear waves. For weakly damped linear wave PDEs (8) with $c_D = 10^{-6}$, $c_V = 0.0001$, Figure 12 illustrate that the macroscale eigenvalues ($\Re(\lambda_p) > -0.01$ and $|\Im(\lambda_p)| < 10$) of the patch scheme #79985 agree exactly with the eigenvalues λ_μ of the staggered full-domain microscale model (3). We now explore all of the 624 stable staggered patch grids, and

the imaginary and real parts of their eigenvalues. First, a plot of imaginary parts of the macroscale eigenvalues for all the 624 stable staggered patch grids for weakly damped linear waves (not included herein) is visually nearly identical to [Figure 10](#) for the ideal wave. Quantitatively, for all 60 centred patch grids, $\Im(\lambda_p)$ agrees to numerical error with $\Im(\lambda_\mu)$ of the full-domain microscale model. But none of the 564 non-centred patch grids $\Im(\lambda_p)$ agree with all the $\Im(\lambda_\mu)$. Secondly, [Figure 13](#) plots the real parts of the macroscale eigenvalues (red dots and blue circles) for all the 624 stable staggered patch grids ([Figure 7](#)) that contain only symmetric patches $uuvv$, $hhvv$, $uuhh$, and $hhhh$ from [Figure 2b](#) or an empty patch. In [Figure 13](#), the horizontal black lines correspond to $\Re(\lambda_\mu)$ from the eigenvalues (10) for macroscale wavenumbers $k_x, k_y = 0, \pm 1, \pm 2$ with $\delta = 2\pi/300$. [Figure 13](#) illustrates that for all 60 centred patch grids, $\Re(\lambda_p)$ (blue circles) agree exactly with $\Re(\lambda_\mu)$ (black lines) of full-domain microscale model (3) (within numerical roundoff errors). On the other hand, for none of the 564 non-centred patch grids do all $\Re(\lambda_p)$ (red dots) agree with the $\Re(\lambda_\mu)$ (black lines). That is, just as for ideal waves, *for weakly damped linear waves, all the 60 centred staggered patch grids give accurate patch schemes, but none of the stable non-centred patch grids are accurate.*

All the accuracy studies reported in the preceding paragraphs of this subsection are for $n = 6$ sub-patch micro-grid intervals, which are representative of the staggered patch grids with odd $n/2$. A similar study for $n = 4$ (not included herein), as a representative of patch grids with even $n/2$, also confirms that among the 83 520 possible 2D staggered patch grids only the 60 centred staggered patch grids give accurate patch schemes. Thus, among *all these possible 167 040 compatible 2D staggered patch grids, only 120 centred patch grids (0.07%) are both stable and accurate.*

5 Conclusion

Accurate numerical simulation of wave-like systems is challenging, especially over long simulation times. Such challenges become even more intricate for large-scale simulations reliant on modelling small-scale features, especially in multiple dimensions. For wave-like systems in full-domain modelling, a common strategy for accurate and robust numerical schemes is to use staggered grids ([Section 2](#)). For high accuracy and to preserve much of the wave characteristics, *this article extends the concept of staggered grids in full-domain modelling to multidimensional multiscale modelling* ([Section 3](#)). We developed and analysed all the possible 167 040 2D staggered patch grids that are *geometrically compatible* for wave-like systems ([Section 3.2](#)).

For first-order PDEs, the patch schemes over these staggered patch grids interpolate field values to the patch edges. However, higher-order spatial derivatives (e.g., for diffusion) and some nonlinear terms require interpolation of additional layers of edge values (Section 3.3). Extending to higher dimensions should be straightforward.

Almost all such multiscale staggered patch grids lead to unstable and/or inaccurate equation-free multiscale patch schemes. We identified 120 staggered patch grids that constitute stable and accurate multiscale schemes. For representative physical and discretisation parameters, via eigenvalues and wave frequencies, we demonstrate the stability, accuracy, and wave-preserving characteristic of the centred multiscale staggered grids for weakly damped linear waves (Section 4). The geometry-stability study (Section 4.2) shows that among all the compatible 167 040 compatible patch grids, only 1248 patch grids (0.75%) whose patches are all symmetric are stable. None of the non-centred patch grids that are stable (Section 4.2) is accurate (Section 4.3). Thus, among all the possible 167 040 compatible 2D staggered patch grids, only 120 centred patch grids (0.07%) are both stable and accurate.

This article develops 120 centred multiscale staggered grids and demonstrates their stability, accuracy, and wave-preserving characteristic for multiscale modelling of weakly damped linear waves for representative physical and discretisation parameters. But most characteristics of the developed multiscale staggered grids must also hold in general for multiscale modelling of many complex spatio-temporal physical phenomena such as the general computational fluid dynamics.

Our next article on multiscale simulation of large-scale linear waves explores two families of patch schemes of Section 3.1 in greater detail over a wider range of parameters for their stability, accuracy, consistency, and their practical insensitivity to numerical roundoff errors. Subsequent articles will explore staggered patch schemes for nonlinear wave PDEs, specifically for viscous thin fluid flows and for turbulent shallow water flows.

References

- Altmann, Robert, Patrick Henning, and Daniel Peterseim (May 2021). "Numerical homogenization beyond scale separation". In: *Acta Numerica* 30, pp. 1–86. ISSN: 0962-4929, 1474-0508. DOI: [10.1017/S0962492921000015](https://doi.org/10.1017/S0962492921000015) (cit. on p. 3).
- Anderson, John D. (1995). *Computational fluid dynamics*. McGraw-Hill. ISBN: 0070016852 (cit. on p. 2).

- Arakawa, Akio and Vivian R. Lamb (1977). “Computational Design of the Basic Dynamical Processes of the UCLA General Circulation Model”. In: *General Circulation Models of the Atmosphere*. Vol. 17. Methods in Computational Physics: Advances in Research and Applications. Elsevier, pp. 173–265. DOI: [10.1016/B978-0-12-460817-7.50009-4](https://doi.org/10.1016/B978-0-12-460817-7.50009-4) (cit. on p. 4).
- Bunder, J. E., J. Divahar, I. G. Kevrekidis, Trent W. Mattner, and A.J. Roberts (2020). “Large-scale simulation of shallow water waves via computation only on small staggered patches”. In: *International Journal for Numerical Methods in Fluids*. DOI: [10.1002/flid.4915](https://doi.org/10.1002/flid.4915) (cit. on pp. 8, 9).
- Bunder, J. E., I. G. Kevrekidis, and A. J. Roberts (July 2021). “Equation-free patch scheme for efficient computational homogenisation via self-adjoint coupling”. In: *Numerische Mathematik* 149.2, pp. 229–272. DOI: [10.1007/s00211-021-01232-5](https://doi.org/10.1007/s00211-021-01232-5) (cit. on p. 8).
- Bunder, J. E., A. J. Roberts, and I. G. Kevrekidis (2017). “Good coupling for the multiscale patch scheme on systems with microscale heterogeneity”. In: *Journal of Computational Physics* 337, pp. 154–174. DOI: [10.1016/j.jcp.2017.02.004](https://doi.org/10.1016/j.jcp.2017.02.004) (cit. on pp. 3, 9).
- Cao, M. and A. J. Roberts (2013). “Multiscale modelling couples patches of wave-like simulations”. In: *ANZIAM Journal* 54, pp. C153–C170. DOI: [10.21914/anziamj.v54i0.6137](https://doi.org/10.21914/anziamj.v54i0.6137) (cit. on p. 3).
- (2015). “Multiscale modelling couples patches of non-linear wave-like simulations”. In: *IMA Journal of Applied Mathematics* 81.2, pp. 228–254. DOI: [10.1093/imamat/hxv034](https://doi.org/10.1093/imamat/hxv034) (cit. on pp. 3, 8).
- (June 2016). “Modelling suspended sediment in environmental turbulent fluids”. In: *Journal of Engineering Mathematics* 98.1, pp. 187–204. DOI: [10.1007/s10665-015-9817-7](https://doi.org/10.1007/s10665-015-9817-7) (cit. on p. 19).
- Dean, Robert G and Robert A Dalrymple (1991). *Water Wave Mechanics for Engineers and Scientists*. World Scientific. DOI: [10.1142/1232](https://doi.org/10.1142/1232) (cit. on pp. 5, 18).
- Divahar, J. (2022). “Accurate multiscale simulation of wave-like systems”. PhD thesis. School of Mathematical Sciences, University of Adelaide (cit. on p. 34).
- Efendiev, Y., Thomas Y. Hou, and V. Ginting (2004). “Multiscale Finite Element Methods for Nonlinear Problems and Their Applications”. In: *Commun. Math. Sci.* 2.4, pp. 553–589. URL: <http://projecteuclid.org/euclid.cms/1109885498> (cit. on p. 3).
- Fish, Jacob, Gregory J. Wagner, and Sinan Keten (June 2021). “Mesoscopic and multiscale modelling in materials”. In: *Nature Materials* 20.6, pp. 774–786. ISSN: 1476-4660. DOI: [10.1038/s41563-020-00913-0](https://doi.org/10.1038/s41563-020-00913-0) (cit. on p. 3).

- Foias, C., M. S. Jolly, I. G. Kevrekidis, G. R. Sell, and E. S. Titi (1988a). "On the computation of inertial manifolds". In: 131.7, pp. 433–436. ISSN: 0375-9601. DOI: [10.1016/0375-9601\(88\)90295-2](https://doi.org/10.1016/0375-9601(88)90295-2) (cit. on p. 9).
- Foias, C., G. R. Sell, and R. Temam (1988b). "Inertial manifolds for nonlinear evolutionary equations". In: *Journal of Differential Equations* 73.2, pp. 309–353. DOI: [10.1016/0022-0396\(88\)90110-6](https://doi.org/10.1016/0022-0396(88)90110-6) (cit. on p. 9).
- Fornberg, Bengt (1990). "High-Order Finite Differences and the Pseudospectral Method on Staggered Grids". In: *SIAM Journal on Numerical Analysis* 27.4, pp. 904–918. DOI: [10.1137/0727052](https://doi.org/10.1137/0727052) (cit. on p. 4).
- Fornberg, Bengt and Michelle Ghrist (1999). "Spatial Finite Difference Approximations for Wave-Type Equations". In: *SIAM Journal on Numerical Analysis* 37.1, pp. 105–130. DOI: [10.1137/S0036142998335881](https://doi.org/10.1137/S0036142998335881) (cit. on p. 4).
- Griffiths, Graham W. and William E. Schiesser (2011). *Traveling Wave Analysis of Partial Differential Equations: Numerical and Analytical Methods with Matlab and Maple*. 1st ed. Academic Press. ISBN: 9780123846525. DOI: [10.1016/C2009-0-64536-0](https://doi.org/10.1016/C2009-0-64536-0) (cit. on p. 22).
- Harlow, Francis H. and J. Eddie Welch (1965). "Numerical Calculation of Time-Dependent Viscous Incompressible Flow of Fluid with Free Surface". In: *The Physics of Fluids* 8.12, pp. 2182–2189. DOI: [10.1063/1.1761178](https://doi.org/10.1063/1.1761178) (cit. on p. 4).
- Hinch, E. J. (2020). *Think Before You Compute*. Cambridge University Press. ISBN: 978-1-10847954-7. DOI: [10.1017/9781108855297](https://doi.org/10.1017/9781108855297) (cit. on pp. 2, 22).
- Hyman, J. M. (May 2005). "Patch dynamics for multiscale problems". In: *Computing in Science Engineering* 7.3, pp. 47–53. DOI: [10.1109/MCSE.2005.57](https://doi.org/10.1109/MCSE.2005.57) (cit. on p. 8).
- Kevrekidis, I. G., C. W. Gear, and G. Hummer (2004). "Equation-free: The computer-aided analysis of complex multiscale systems". In: *AIChE Journal* 50.7, pp. 1346–1355. DOI: [10.1002/aic.10106](https://doi.org/10.1002/aic.10106) (cit. on pp. 8, 9).
- Kevrekidis, I. G. and G. Samaey (2009). "Equation-Free Multiscale Computation: Algorithms and Applications". In: *Annual Review of Physical Chemistry* 60.1, pp. 321–344. DOI: [10.1146/annurev.physchem.59.032607.093610](https://doi.org/10.1146/annurev.physchem.59.032607.093610) (cit. on pp. 3, 8).
- Lauritzen, Peter, Christiane Jablonowski, Mark Taylor, and Ramachandran Nair (2011). *Numerical Techniques for Global Atmospheric Models*. Springer. DOI: [10.1007/978-3-642-11640-7](https://doi.org/10.1007/978-3-642-11640-7) (cit. on pp. 4, 5).
- LeVeque, Randall J. (2015). "Tsunami modelling". In: *Princeton Companion to Applied Mathematics*. Ed. by Nicholas J. Higham, Mark R. Dennis, Paul Glendinning, Paul A. Martin, Fadil Santosa, and Jared Tanner. Princeton. Chap. V.19, pp. 712–720 (cit. on p. 4).

- Lorenz, E. N. (1986). "On the Existence of a Slow Manifold". In: *Journal of the Atmospheric Sciences* 43.15, pp. 1547–1558. DOI: [10.1175/1520-0469\(1986\)043<1547:OTE0AS>2.0.CO;2](https://doi.org/10.1175/1520-0469(1986)043<1547:OTE0AS>2.0.CO;2) (cit. on p. 9).
- Maclean, J., J. E. Bunder, and A. J. Roberts (Aug. 2021). "A toolbox of equation-free functions in Matlab/Octave for efficient system level simulation". In: *Numerical Algorithms* 87.4, pp. 1729–1748. DOI: [10.1007/s11075-020-01027-z](https://doi.org/10.1007/s11075-020-01027-z) (cit. on pp. 3, 9).
- Mehaute, Bernard Le (1976). *An Introduction to Hydrodynamics and Water Waves*. 1st ed. Springer Study Edition. Springer Berlin Heidelberg. ISBN: 9783642855696. DOI: [10.1007/9783642855672](https://doi.org/10.1007/9783642855672) (cit. on pp. 5, 18).
- Ólafsson, Haraldur and Jian-Wen Bao (2021). *Uncertainties in Numerical Weather Prediction*. Elsevier. ISBN: 9780128154915. DOI: [10.1016/C2017-0-03301-3](https://doi.org/10.1016/C2017-0-03301-3) (cit. on pp. 4, 5).
- Patankar, S.V and D.B Spalding (1972). "A calculation procedure for heat, mass and momentum transfer in three-dimensional parabolic flows". In: *International journal of heat and mass transfer* 15.10, pp. 1787–1806 (cit. on p. 4).
- Rackauckas, Christopher and Qing Nie (2017). "DifferentialEquations.jl—a performant and feature-rich ecosystem for solving differential equations in julia". In: *Journal of Open Research Software* 5.1. DOI: [10.5334/jors.151](https://doi.org/10.5334/jors.151) (cit. on p. 9).
- Reungoat, David, Pierre Lubin, Xinqian Leng, and Hubert Chanson (Oct. 2018). "Tidal bore hydrodynamics and sediment processes: 2010–2016 field observations in France". In: *Coastal Engineering Journal* 60.4, pp. 484–498. ISSN: 2166-4250. DOI: [10.1080/21664250.2018.1529265](https://doi.org/10.1080/21664250.2018.1529265) (cit. on p. 4).
- Roberts, A. J. (1988). "The application of centre-manifold theory to the evolution of system which vary slowly in space". In: *The Journal of the Australian Mathematical Society. Series B. Applied Mathematics* 29.4, pp. 480–500. DOI: [10.1017/S0334270000005968](https://doi.org/10.1017/S0334270000005968) (cit. on p. 9).
- (2003). "Low-Dimensional Modelling of Dynamical Systems Applied to Some Dissipative Fluid Mechanics". In: *Nonlinear Dynamics: From Lasers to Butterflies*, pp. 257–313. DOI: [10.1142/9789812791252_0007](https://doi.org/10.1142/9789812791252_0007) (cit. on p. 9).
- Roberts, A. J. and I. G. Kevrekidis (2005). "Higher order accuracy in the gap-tooth scheme for large-scale dynamics using microscopic simulators". In: *ANZIAM Journal* 46, pp. 637–657. URL: <https://journal.austms.org.au/ojs/index.php/ANZIAMJ/article/view/981> (cit. on pp. 3, 8, 9).

- (2007). “General Tooth Boundary Conditions for Equation Free Modeling”. In: *SIAM Journal on Scientific Computing* 29.4, pp. 1495–1510. DOI: [10.1137/060654554](https://doi.org/10.1137/060654554) (cit. on pp. 3, 8, 9).
- Roberts, A. J. and Zhenquan Li (2006). “An accurate and comprehensive model of thin fluid flows with inertia on curved substrates”. In: *Journal of Fluid Mechanics* 553, pp. 33–73. DOI: [10.1017/S0022112006008640](https://doi.org/10.1017/S0022112006008640) (cit. on p. 19).
- Temam, R. (Sept. 1990). “Inertial manifolds”. In: *The Mathematical Intelligencer* 12.4, pp. 68–74. DOI: [10.1007/BF03024036](https://doi.org/10.1007/BF03024036) (cit. on p. 9).
- Zagaris, Antonios, C. William Gear, Tasso J. Kaper, and I. G. Kevrekidis (2009). “Analysis of the accuracy and convergence of equation-free projection to a slow manifold”. In: *ESAIM: Mathematical Modelling and Numerical Analysis* 43.4, pp. 757–784. DOI: [10.1051/m2an/2009026](https://doi.org/10.1051/m2an/2009026) (cit. on p. 9).
- Zikanov, Oleg (2010). *Essential Computational Fluid Dynamics*. Wiley. ISBN: 9780470423295 (cit. on p. 2).